Sustainable Water Resources Management (2022) 8:104
https://doi.org/10.1007/s40899-022-00684-3

ORIGINAL ARTICLE

Assessment of water supply and demand in Gilgel Gibe watershed, southwest Ethiopia

Sewmehon Sisay Fanta[1] · Wanna Geyisa Namara[1] · Mamuye Busier Yesuf[1]

Received: 2 September 2021 / Accepted: 4 June 2022

Abstract

Integrated water resource management requires reliable information on the available water resources and demand. This study aims to assess the future water supply and demand under the combined effect of climate change and socio-economic scenarios using the HEC-HMS and WEAP model for the Gilgel Gibe watershed. The required spatial, hydro-metrological, and socio-economic data were directly collected from different organizations. The precipitation and temperature data forecasted by regional climate models under representative concentration pathway 4.5 were used to simulate the stream flow using the HEC-HMS model. The unmet demand from 2019 to 2050 was estimated under socio-economic scenarios. The result shows that the reference scenario increased annually by 206 million cubic meters (MCM). Similarly, the unmet demand under the Irrigation Area Expansion (IAE) scenario increased at an annual rate of 90 MCM, the maximum increment rate among all scenarios. However, the annual unmet demand under the New Irrigation Technology (NIT) scenario shows a reduction of 0. 3MCM. The IAE scenario also showed a power production reduction of the Gilgel Gibe hydropower plant I by 12% compared to the reference scenario. However, the power production capacity increased by 15.27% under the NIT scenario. The result indicates that socio-economic scenarios are more responsible than climate change scenarios for the occurrence of water scarcity. Therefore, efficiency maximization-based water resource planning should be implemented to minimize the water scarcity problems. In this regard, the study has valuable information which can aid water resource planners for wise use of decision-making.

Keywords Climate change · Gilgel Gibe watershed · HEC-HMS · Scenario · Unmet demand · WEAP

Introduction

Climate change affected the local and global hydrologic cycle (Touseef et al. 2021). However, the impact of climate change varies from place to place throughout the world. For example, some basins show an increment of flow leading to high floods, whereas others show a reduction of flow with intensified drought (Pousa et al. 2019). According to the Intergovernmental Panel on Climate Change (IPCC) and Food Agriculture Organization (FAO), the effect of climate change, even under the optimistic scenario, will not be minimized to the required level (Amin et al. 2018). Consequently, it is expected that the world water demand will increase by 55% in 2050 (Silva et al. 2020). This is due to climate change, urbanization, and unexpected increment in the world population. There is also increasing competition for water with other sectors. However, the agriculture sector will be the most susceptible in developing countries. Because, the socio-economic economic activities of developing countries are largely dependent on agriculture. Hence, the combined effect of population growth, climate change, and unlimited human need will force progressive pressure on the available water resource, which may cause the continuous decline of the available water resources in the future (Agarwal et al. 2019; Alemu and Dioha 2020; Silva et al. 2020). Population increment, urban expansion, agricultural activities, and improvement of the living standard of the society are the major socio-economic activities that affect the water consumption rate. Therefore, understanding the future trend of sectoral water demand aids to develop efficient water resources management scenario that will compromise the impact of climate change and socio-economic activities (Amin et al. 2018; Silva et al. 2020). Therefore, it

✉ Sewmehon Sisay Fanta
sewmehonsisay@gmail.com

[1] Faculty of Civil and Environmental Engineering, Jimma University, Jimma, Ethiopia

Published online: 02 July 2022

is necessary to quantify the impact of climate change and the spatiotemporal dynamics of water demand.

In Ethiopia, the uneven spatial and temporal occurrence and distribution of the water resources have been considered the major factors affecting the development and management of the country's water sector (Seleshi and Zanke 2004; Cheung et al. 2008). The Gilgel Gibe watershed is part of the Omo-Gibe basin located in southwestern Ethiopia. The community's estimated population that lives in the watershed at the end of 2019 was 2,074,117. Currently, the ecosystem of the watershed has shown a rapid temporal variation. Deforestation, over-grazing, burning wood, expansion of farming, and poor land management are the main anthropogenic activities that have severely degraded the ecosystem of the Gilgel Gibe watershed. Due to this, the local climate caused seasonal rainfall shifts, increment of temperature (Fanta 2022), flash floods, drought, reduction and fluctuation of hydropower production, and reduction of stream flow capacity (Teklu et al. 2016). The problems are not limited to the Gilgel Gibe watershed. It is the whole part of Ethiopia.

The Gilgel Gibe Hydropower plant I, with an annual power production capacity of 184 MW, is located in the Gilgel Gibe watershed. Downstream of the Gilgel Gibe I hydropower plant, there is a Gilgel Gibe II hydropower plant with a capacity of 420 MW. The water source of these hydropower plants is the Gilgel Gibe River. The Gilgel Gibe River is also the largest tributary of the Omo_Gibe River. The lower reach of the Omo-Gibe River is being developed for agricultural activities that cover 175,000 ha of land for the production of sugarcane. Increment in evaporation, sediment yield, and flooding are the major climate change extremes that affect the production capacity of the Gibe I and Gibe II hydropower plants. Therefore, climate change has made power production more variable and uncertain.

The overall impact of climate change, expansion of development activities, and unlimited population increment have caused a continuous increase in water demand that put pressure on the available water resources of the watershed. On the other hand, the future water resource availability and priorities on water resource allocation and improvement of society's socio-economic status are not considered during the design of water resource projects (Jillo et al. 2017). Consequently, many water resource projects failed before their useful life. Power interruption is also common in years of severe drought in Ethiopia. For example, the 2008–2009 droughts caused a power interruption that lasted for about 4 months with a 1-day-per-week complete interruption throughout the country, obstructing all business and economic activities. Even though, the water demand is increasing under limited water resources, the climate change impacts and the level of vulnerability are not yet sufficiently addressed in the water resources of the Gilgel Gibe watershed. Therefore, a study is needed to quantify future water resources and socio-economic demand for efficient water resources and watershed management. Hence, this study aims to quantify the water supply and demand of the Gilgel Gibe watershed under climate change and socio-economic scenarios using the HEC-HMS and WEAP model.

In literature, there are different types of water resource allocation tools. For example, the Catchment Water Allocation Tool (CaWAT) is used for water resource allocation within a demand node based on the water balance. The Resource Allocation Model (REALM) is a comprehensive tool used for the bulk distribution of water resources allocation within the water supply system (Amin et al. 2018). It is more flexible and widely used for water supply planning and management. The Modular Simulator (MODSIM) is also a river basin management tool for short-term and long-term operational planning and water right analysis (Emami and Koch 2018). The Multi-Objective Programming (MOP) model is used for water resources allocation and conflict resolution between different demand sectors for the unshared basin (Roozbahani et al. 2015). The model maximizes both the satisfaction of water demand and the economic benefit gained from the demand sector. The AQUATOOL is used for water resource allocation and analysis of alternative approaches for water resource management (Pedro-Monzonís et al. 2016).

The WEAP model is a computer simulation package used for water resource allocation under various demand and management scenarios (Gedefaw et al. 2019). It is a microprocessor tool developed by Stockholm Environment Institute (SEI) for water demand and supply analysis under user-specified management policy (Tena et al. 2019). The model is a comprehensive, flexible, straightforward, and user-friendly framework for scenario analysis of multiple and competing uses of water resource systems (Li et al. 2015). It is a priority-driven software that employs a priority-based optimization algorithm using the concept of equity group to allocate water during inadequate supply (Olabanji et al. 2020). The WEAP model was successfully applied by several researchers throughout the world for water resource allocation at basin and watershed scale under the impact of climate change and socio-economic activities (Dong et al. 2013; Mourad and Alshihabi 2016; Amin et al. 2018; Olabanji et al. 2020; Touseef et al. 2021). In Ethiopia, Adgolign et al. (2016); Gedefaw et al. (2019); Alemu and Dioha (2020); Abera Abdi and Ayenew (2021) applied the WEAP model for water resource allocation under climate change, domestic, and irrigation water demand scenarios. Operating policies in the WEAP model are more flexible and user-friendly that allow resources maximization based on best management scenarios (Olabanji et al. 2020). Therefore, this study applied the WEAP model to quantify the future water demand under the available future water resources for the Gilgel Gibe watershed. Easily and cost-free availability of

the WEAP model, its flexibility, user-friendly, operation of the model based on the available data, and successfulness of the model in wider applicably by several scholars throughout the world, including Ethiopia, are some of the main criteria to select the WEAP model.

WEAP model operates the water supply and demand based on the mass balance equation (Abera Abdi and Ayenew 2021). The future water demand depends upon future water resource potential availability. Therefore, it is necessary to forecast the quantity of water under the impact of climate change. Distributed hydrological models varying from lumped to fully distributed models are widely used to estimate the watershed runoff potential (Pechlivanidis et al. 2011). The selection of hydrological models is based on the data availability, affordability, and project objective. HEC-HMS is a semi-distributed hydrological model developed by the United States Army Corps of Engineers (USACE). It is used for continuous and event-based runoff simulation. Several researchers approved the successfulness of the HEC-HMS model in runoff simulation in various parts of the world under various watershed characteristics (Halwatura and Najim 2013; Gebre 2015; Zelelew and Melesse 2018; Tassew et al. 2019; Fanta and Feyissa 2021). Therefore, the HEC-HMS was applied for the runoff simulation of the Gilgel Gibe watershed for the study.

Materials and methods

Description of the study area

Gilgel Gibe watershed is located southwest of Ethiopia in the Oromiya regional state. The watershed has an area of 4225 Km^2. The elevation ranges between 1096 and 3259 m.a.s.l. Figure 1 shows the location map of the Gilgel Gibe watershed.

The watershed has three major climate regions. These are: subtropical, temperate, and tropical ecology, covering about 78, 12, and 10%, respectively. The tropical agro-climate is located in Limmu Seka, Sekoru, Dedo, and Seka Chekorsa. However, Manna and Tiro Afeta belong to the subtropical agro-climate, whereas Omo Nada, Kersa, and Limmu Seka are categorized under temperate agro-climate regions.

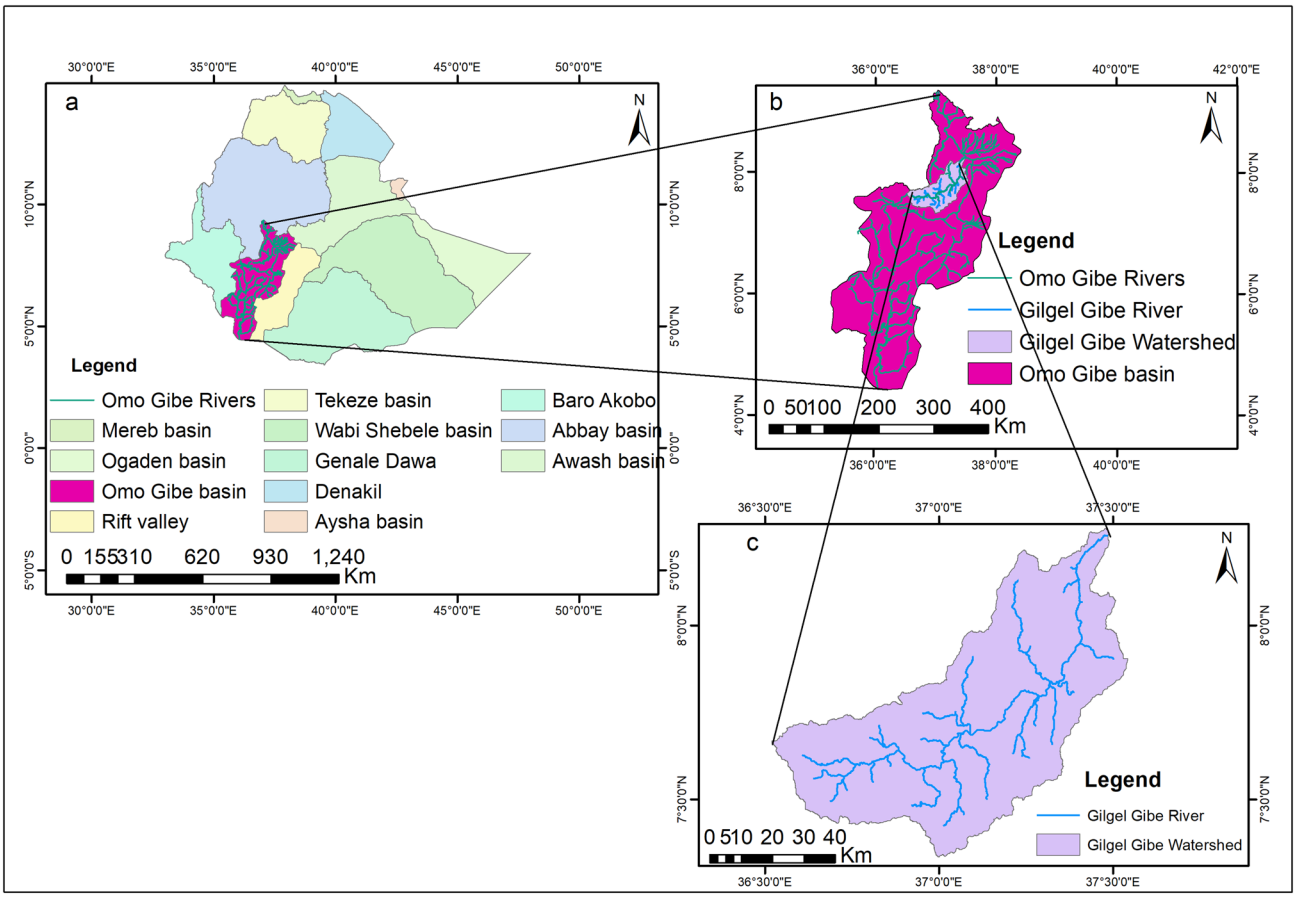

Fig. 1 Location map of the study area

The watershed is weakly bimodal rainfall with spring a short rainy season during April and May, while summer (June, July, and August) is a long rainy season. The rainfall and temperature vary spatially due to the undulating topography of the watershed. The observed precipitation analysis indicates that the watershed has an average rainfall that varies from 1300 to 1700 mm and an average temperature varying from 20 to 23 °C. Jaweso et al. (2019) studied the metrological trend of the upper Omo-Gibe basin, including the Gilgel Gibe watershed from 1981 to 2008. The finding showed that the mean annual rainfall showed decreasing trends. In contrast, temperature showed a significant level of increment.

Agriculture is the dominant livelihood and income source of the watershed. Recently, more than 91% of the watershed has been extensively cultivated. The agro-climatic conditions of the watershed make it suitable for producing permanent crops (coffee and fruits) and annual crops (cereals, pulses, and oilseeds). However, in Ethiopia, climate change has caused a reduction in crop production and intensification of crop diseases and pests due to high moisture evaporation from the crop and the soil surface, increasing the water consumption rate (Bekele et al. 2017; Asfaw et al. 2018; Bayable et al. 2021).

Method

Data collection and analysis, future stream flow simulation, water demand forecasting, and analysis under different scenarios are the main procedures to achieve the study's objective. Figure 2 shows the simplified representation of the study design. The main source of drinking water supply for the Gilgel Gibe watershed community is the Gilgel Gibe River. Therefore, the population is the main driving factor of water demand. Therefore, the watershed's population under different growth rates was included during the water demand computation.

Data collection

Spatial and observed hydro-metrological data, RCMs' data, reservoir data, and socio-economic data were the major data type used for this study. Table 1 shows the datasets and their sources. The daily stream flow data from 1985 to 2005 were used for the HEC-HMS model calibration and validation.

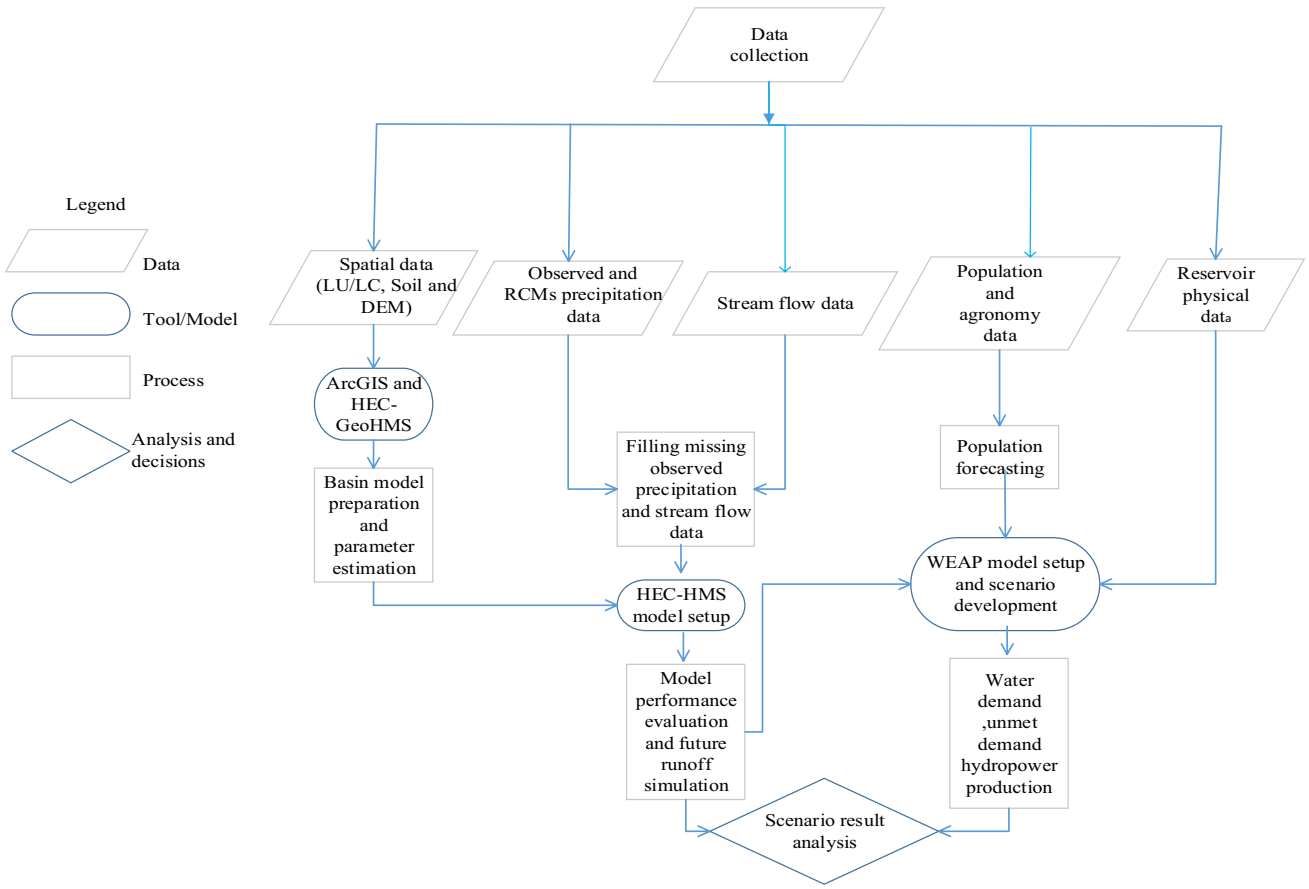

Fig. 2 Conceptual framework of the study

Table 1 Datasets and sources

Data type	Sources
Observed precipitation	National Metrological Agency of Ethiopia (NMAE)
Stream flow	Hydrology Department of Ministry of Water, Irrigation, and Electricity (MoWIE)
Climate data	ESGF-CORDEX-Africa database
LU/LC and soil data	GIS department of MoWIE
DEM (12.5 m × 12.5 m resolution)	Alaska Satellite Facility Service (http://www.vertex.daac.asf.Alaska)
Reservoir data	Ethiopian Electric Power Corporation (EEPCO) and MoWIE
Socio-economic data	Jimma zone finance and economic cooperation office
Irrigation data (irrigation area, soil type, irrigation efficiency, crop types, and crop growth period)	Jimma zone irrigation authority office

Crop production and crop export index are the major factors that affect the water consumption rate. However, the water consumption rate depends on the crop type, growth period, and irrigation area covered by each crop type. Therefore, these data were used to quantify the annual crop water demand.

Among the existing weather stations near and inside the watershed, Shebe, Dedo, Omo_Nada, Limu_Genet, and Sekoru stations were selected based on the availability of minimum missing data. The summary information of the selected meteorological stations is demonstrated in Table 2.

Precipitation data analysis

The observed precipitation has missing rainfall ranging from 2.5% to 10% of the observed data (Table 2). The predictive mean match and linear regression methods in Statistical Package for Social science (SPSS) tool were used to fill the missing data. The Standard Normal Homogeneity Test (SNHT) was used to detect a break in the trend of the observed data due to the location of the gauge, LU/LC change, observational errors, and wind effect. The analysis showed that all the precipitation data are homogeneous, because there is no gauge location change. Moreover, only two of the five stations (Dedo and Shebe) are ordinary stations, whereas the remaining are principal stations.

The historical and future projected weather data for the Coordinated Regional Climate Downscaling Experiment (CODEX) under the African database for CCLM4, HIRHAM5, and RACMO22T were downloaded in the form of an NETCDF file. The projected precipitation and temperature by RCMs were used to simulate the runoff of the Gilgel Gibe watershed.

The point observed and RCM precipitation were converted into areal rainfall using the Thiessen polygon. Even though this method does not consider the effect of topography and wind on areal rainfall distribution, it has been selected due to the proportional distribution of gauging stations in and around the watershed. Thus, each sub-watershed (SW) received daily rainfall from the gauging station according to the gauge weight. Table 3 shows the precipitation contributing stations and grid points (GPs) for each sub-watershed. Figure 3 also shows the location of each gauging station and (GPs).

HEC-HMS model setup

HEC-HMS is a semi-distributed hydrological model used designed for continuous and event-based runoff simulation. Detail descriptions of the model are available in Halwatura and Najim (2013), Gebre (2015), Skhakhfa and Ouerdachi (2016), Zelelew and Melesse (2018). For this

Table 2 Summarized information of the selected meteorological stations

S no.	Station name	Latitude (°)	Longitude (°)	Elevation (m)	Duration (year)	Missing data (%)
1	Sekoru	7.92	37.42	1928	1985–2017	9.45
2	Limu Genet	8.07	36.95	1766	1985–2017	7.8
3	Asendabo	7.75	37.22	1764	1985–2017	5.25
4	Jimma	7.7	36.82	1718	1985–2017	2.5
5	Dedo	7.52	36.87	2210	1985–2017	8.5
6	Omo_Nada	7.62	37.25	1838	1985–2017	9.25
7	Shebe	7.5	36.52	1813	1985–2017	10

Table 3 Observed and GPs' SW gauge weight

Gauging stations						Grid point				
SW name	Shebe	Dedo	Omo_Nada	Limu_Genet	Sekoru	GP109211	GP110211	GP111211	GP110212	GP111212
SW1	0.00	0.00	0.00	0.00	1.00	0.00	0.00	0.00	0.00	1.00
SW2	0.00	0.00	0.00	0.00	1.00	0.00	0.00	0.00	0.00	1.00
SW3	0.00	0.15	0.54	0.19	0.12	0.00	0.09	0.02	0.69	0.19
SW4	0.00	0.49	0.51	0.00	0.00	0.00	0.93	0.03	0.05	0.00
SW5	0.37	0.63	0.00	0.00	0.00	0.51	0.39	0.00	0.10	0.00
SW6	0.00	0.00	0.05	0.00	0.00	0.00	1.00	0.00	0.00	0.00
SW7	0.00	0.00	0.68	0.00	0.32	0.00	0.01	0.47	0.00	0.52
SW8	0.00	0.00	0.00	0.18	0.82	0.11	0.00	0.00	0.00	0.89

study, the steps to prepare the subbasin and watershed parameters are as follows: first, the basin model was prepared by the HEC-GeoHMS tool in ArcGIS environment. Next, the curve number grid map for the whole watershed was generated by combining the watershed's soil and LU/LC data. Then, the weighted average curve number values for each sub-watershed and the physical parameters of the subbasin, such as CN, lag time, initial abstraction, wave travel time, and channel storage coefficient, were computed using the HEC-GeoHMS tool. Finally, the basin model and the physical parameters of the watershed were exported to the HEC-HMS model.

The basin model in HEC-HMS has four major analytical components for the hydrological process. These are base flow, loss, transform, and channel routing. The selected methods and the reasons for selecting each method are illustrated in Table 4.

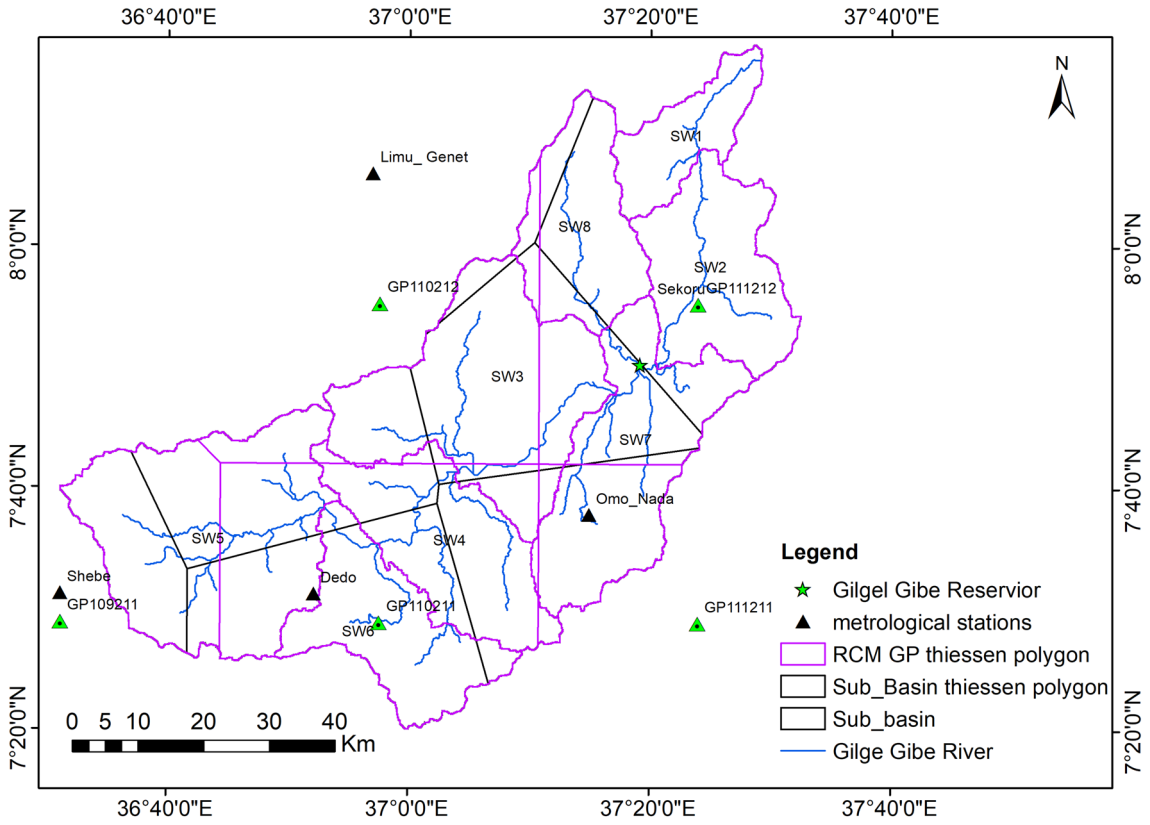

Fig. 3 Thiessen polygon for Gauging station and grid points

Table 4 Selected methods for the computation of major hydrological processes

Hydrological process	Method	Reason
Baseflow	Monthly constant	(1) Availability of initial input parameters (2) Wider applicability (Koneti et al. 2018)
Loss	Initial and constant SCS-CN	(1) Wider applicability (Verma et al. 2010) (2) Appropriateness of the assumptions inherited in the model (3) Availability of initial input parameters
Transform	SCS-UH	(1) Wider applicability (Gyawali and Watkins 2013; Skhakhfa and Ouerdachi 2016) (2) Availability of initial input parameters
Channel routing	Muskingum	(1) Wider applicability (Majidi and Shahedi 2012; Skhakhfa and Ouerdachi 2016) (2) Appropriateness of the assumptions inherited in the model (Fanta and Feyissa 2021) (3) Availability of initial input parameters

Sensitivity analysis, calibration, and validation of the HEC-HMS model

Before the simulation of the future Gilgel Gibe watershed runoff, the optimum values of the watershed parameters were adjusted using HEC-HMS model calibration. Sensitivity analysis was conducted to determine the most sensitive parameter of the watershed. In the HEC-HMS model, sensitivity analysis and model calibration processes are conducted simultaneously. During the sensitivity analysis phase, the initial values of watershed parameters are altered, and runoff simulation is conducted iteratively. Model calibration is the overall process of conducting sensitivity analysis and measuring the simulated and observed runoff hydrograph using different statistical tests of error functions (Fanta and Feyissa 2021). The optimum value of the sensitive parameters was decided when the simulated and observed runoff hydrographs were matched at an acceptable level of accuracy.

Two types of search algorithms are available for parameter adjustment. These are: the univariate gradient (UG) and Nelder and Mead (NM) algorithms. The UG method adjusts one parameter at a time. This method makes successive corrections to obtain the optimal value of the parameter. According to this algorithm, if x^k represents the parameter estimates with the objective function $f(x^k)$ at iteration k, the search defines a new estimate (x^{k+1}) at iteration $k+1$. Mathematically, the UG algorithm is illustrated in Eq. (1)

$$x^{\kappa+1} = x^{\kappa} + \Delta x^{\kappa}, \tag{1}$$

where Δx^{κ} is the correction to the parameter obtained by successive optimization trials using Eq. (2)

$$\Delta x^{\kappa} = 0.01 c x^{k}, \tag{2}$$

where c is a coefficient for correction of the univariate gradient method. The trial will terminate when $f(x^{k+1}) < f(x^k)$.

The NM search algorithm uses downhill simplex to identify the parameter to be adjusted among the given parameters. This algorithm can adjust more than one parameter at a time. The method searches for the optimum value of the watershed parameters without using objective functions. It is based on prior experience of several iteration trials that remove the poor and improve the good parameter estimates. Both the UG and NM methods are dependent on the input parameter's initial values. The poor assumption of the initial parameter value may cause an inappropriate conclusion regarding the optimum parameter value (Kumarasamy and Belmont 2018). Therefore, if a good initial parameter estimation approximates its actual watershed parameter value, the search methods will obtain the optimum value in a small number of optimization trials. For this study, the UG method was selected during sensitivity analysis of the constant rate of infiltration and wave travel time. While, the sensitivity analysis of curve number, lag time, and initial abstraction was conducted using the NM method.

In this study, the HEC-HMS model was calibrated from 1985 to 1999 using daily observed flow data near the watershed outlet. The widely used statistical tests of error functions [Nash and Sutcliff efficiency (NSE), percent bias (Pbias), ratio of root-mean-square error to the standard deviation of the data (RSR), and coefficient of determination (R^2)] were used to compare the simulated and observed runoff hydrographs. The detail descriptions and equations of these statistical metrics are available in Moriasi et al. (2007), Verma et al. (2010), Zou et al. (2003), and Golmohammadi et al. (2014). The calibrated model was validated using the recently observed data from 2000 to 2005. The optimum values of the watershed parameters obtained by the calibration period were used for runoff simulation during the validation period. Then, runoff simulation from 2006 to 2017 was conducted using the RCMs' precipitation and temperature. The simulated runoff was compared with the observed stream

flow using the same statistical tests of error functions that were used during the calibration and validation.

Computation of crop water demand

Climate change altered the distribution and intensity of precipitation and temperature. Chaemiso et al. (2016) stated that due to climate change, temperature showed consistent increment, and precipitation showed an insignificant increasing trend. The combined effect of an insignificant increment in precipitation and a significant temperature increment causes increment of evapotranspiration and crop water requirements. Hence, the study considered the effect of climate change's impact on crop water requirements throughout the study period. The reference evapotranspiration (ETo) was computed using the modified Penman–Monteith equation, available in Allen et al. (2004) using the FAO CROPWAT8.0 software. The result showed that the monthly reference evapotranspiration (ETo) of the current account year was 3.56 mm/month, whereas the average monthly ETo from 2020 to 2050 was 4.43 mm/month/year. The result signifies that the increment of maximum and minimum temperature caused to increase the ETo by 19.6% from the current account year.

The common crop types planted by the communities are coffee, maize, mango, pepper, potato, and sorghum, which are suitable crop types depending on the study area's soil type and climate condition. Therefore, this study computed the crop water requirement (ETc) of the current account year and future period for these crop types. The analysis indicates that the increment of ETo caused the reduction of depth and duration of soil moisture potential. Consequently, the irrigation interval during the future period was shorter than the reference period. The result also showed that the depth of irrigation and flow for the current account year was less than that of the future period. This indicates that the crop water requirements showed a substantial increment for the future period of the study. On the other hand, irrigation frequency is inversely related to the initially available soil moisture depth. As a result, the irrigation interval for the future period was shorter than the irrigation interval for the current account year due to the impact of climate change. Table 5 shows the irrigation date after planting, duration and irrigation intervals after each consecutive irrigation day, the crop water requirement in terms of depth of irrigation (mm), and flow rate (litter/second/hectare).

The annual crop water requirement was computed based on the monthly crop water required by the selected crop. Based on the result, the annual water consumption rate during the current account year was 107,537.76 m^3/ha/year. However, the annual water consumption rate for the future period was 108,483.8 m^3/ha/year. The result showed that the

Table 5 Irrigation scheduling for the current account year and scenario period

Current account year (2019)						Scenario period (2020–2050)					
Irrigation date	Duration (days)	Interval	Stage	Depth of irrigation (mm)	Flow (l/s/ha)	irrigation date	Duration (days)	Interval	Stage	Depth of irrigation (mm)	Flow (l/s/ha)
26-Feb	7	–	Init	113.2	2.67	24-Feb	5	–	Init	114.2	3.78
11-Apr	51	44	Init	95.4	0.36	22-Mar	31	26	Init	102.5	0.65
20-Oct	243	192	Mid	59.9	0.05	26-Apr	66	35	Dev	88	0.42
8-Nov	262	19	End	59.9	0.52	22-Jun	123	57	Dev	68.6	0.2
25-Nov	279	17	End	59.5	0.58	16-Oct	239	116	Mid	57.4	0.08
12-Dec	296	17	End	57.6	0.56	29-Oct	252	13	End	56.7	0.72
29-Dec	313	17	End	57.3	0.56	11-Nov	265	13	End	59.1	0.75
15-Jan	330	17	End	57.7	0.56	23-Nov	277	12	End	58.4	0.8
30-Jan	End		End			5-Dec	289	12	End	60.2	0.83
						17-Dec	301	12	End	61.3	0.84
						28-Dec	312	11	End	56.3	0.85
						9-Jan	324	12	End	60.1	0.83
						21-Jan	336	12	End	59.4	0.82
						30-Jan	End		End		

future annual water consumption rate increased by 0.87% from the water requirement of the current account year.

Description of WEAP model

WEAP is a laboratory for alternative water resource management and development strategies. It is a forecasting and policy analysis tool. WEAP simulates water demand, water supply, storage, pollution generation, and waste discharge from the treatment plant as a forecasting tool. As a policy analysis tool, WEAP simulates the full range of the likely impact of socio-economic development on the demand side and management scenario on the supply side (Shumet and Mengistu 2016; Alemu and Dioha 2020).

WEAP model calculation algorithm

The WEAP model operates the monthly water accounting starting from the first month of the current account year to the last month of last year's scenario based on the mass balance equation. Every node and link in the WEAP schematics has a mass balance equation (Mourad and Alshihabi 2016; George Marcellus Metobwa 2018; Abera Abdi and Ayenew 2021). The WEAP model simulates the spatiotemporal distribution of unmet demand coverage and water balance for each demand node using an IP solver, the non-commercial mixed-integer linear programming solver (Agarwal et al. 2019; Bouznad et al. 2020). The model solves allocation problems to maximize demand satisfaction using supply resources and priorities-related constraints. The annual water demand at each demand site can be computed using Eq. (3)

$$AD_{DS} = TAL_{Br} \times WCR_{Br}, \tag{3}$$

where AD is the annual demand (m^3); DS represents the irrigation area and domestic demand site for each district; TAL represents the total activity level which is the irrigation area and total population of each district; Br represents the demand node branch level; WCR represents the water consumption rate (m^3/p/year) for domestic water demand and irrigation water demand (m^3/ha/year). The annual unmet demand is the difference between annual demand and annual supply. Therefore, a portion of water will return to the river downstream of the demand site. This is because the crop water withdrawn from the river is not 100% consumed

$$RF = 1 - CR, \tag{4}$$

where RF represents return flow (%); CR represents the consumption rate (%).

Thus, each irrigation demand site can withdraw water from the Gilgel Gibe River, consume some, and return the residual to the Gilgel Gibe River. The return flow from the irrigation area is mainly dependent on the salinity of the soil, irrigation scheme, infiltration rate, water management, and overall efficiency of the irrigation scheme. However, an accurate estimation of return flow requires a detailed investigation of the infiltration capacity and soil salinity (Wu et al. 2019). In this study, it is expected that 95% of the water is diverted into the irrigation field, considering the amount of water lost due to evaporation, infiltration, and leaching. Hence, 5% of the diverted water is assumed to return to the Gilgel Gibe River. This return flow is available for use in the same month by the downstream demand site.

Hydropower generation was computed from the flow passing through the turbine, based on the reservoir release. Hence, the turbine's maximum flow capacity constrains it. For reservoirs located in the river, all water released downstream is sent through the turbines. The maximum turbine flow bounds the volume of water that passes through the turbines. The amount of energy produced in a certain month can be expressed in Eq. (5)

$$Energy_m = Volume_m \times \eta, \tag{5}$$

where $Energy_m$ is the monthly energy (GJH); $Volume_m$ is the monthly volume of water passing through the turbine (flow rate); η is the generating efficiency of the power plant. The energy produced from the hydropower plant is a function of the mass of water (1000 kg/m^3) through the turbines, operating head (m), the plant factor, and the generating efficiency. The turbine's monthly operating head (drop elevation) is given by Eq. (6)

$$\begin{aligned} \text{Drop elevation } (H) = {} & \text{Begining month elevation}(H) \\ & - \text{Tail water elevation } (H). \end{aligned} \tag{6}$$

WEAP model setup

Schematization, input data, result, and scenario analysis are the basic model setup modules in the WEAP model. Schematization is the first task in the WEAP model where rivers, demand sites, transmission links, reservoirs, and any necessary schematics are added to the WEAP model. For this study, the shape file of the Gilgel Gibe watershed, which was prepared in the HEC-GeoHMS tool with ArcGIS software, was added to the WEAP model. 17 demand nodes, 9 for domestic demand nodes, and 8 for irrigation demand nodes were created in the schematic module of the WEAP model. The demand nodes are directly linked to the supply sources using transmission links. Therefore, 17 transmission links were created that connect the demand node to the supply source. The return flow from the domestic demand is insignificant. Therefore, only the return flow irrigation area was considered. Eight return flows will carry the irrigation demand node to the Gilgel Gibe River. Figure 4 shows the layout of the schematics.

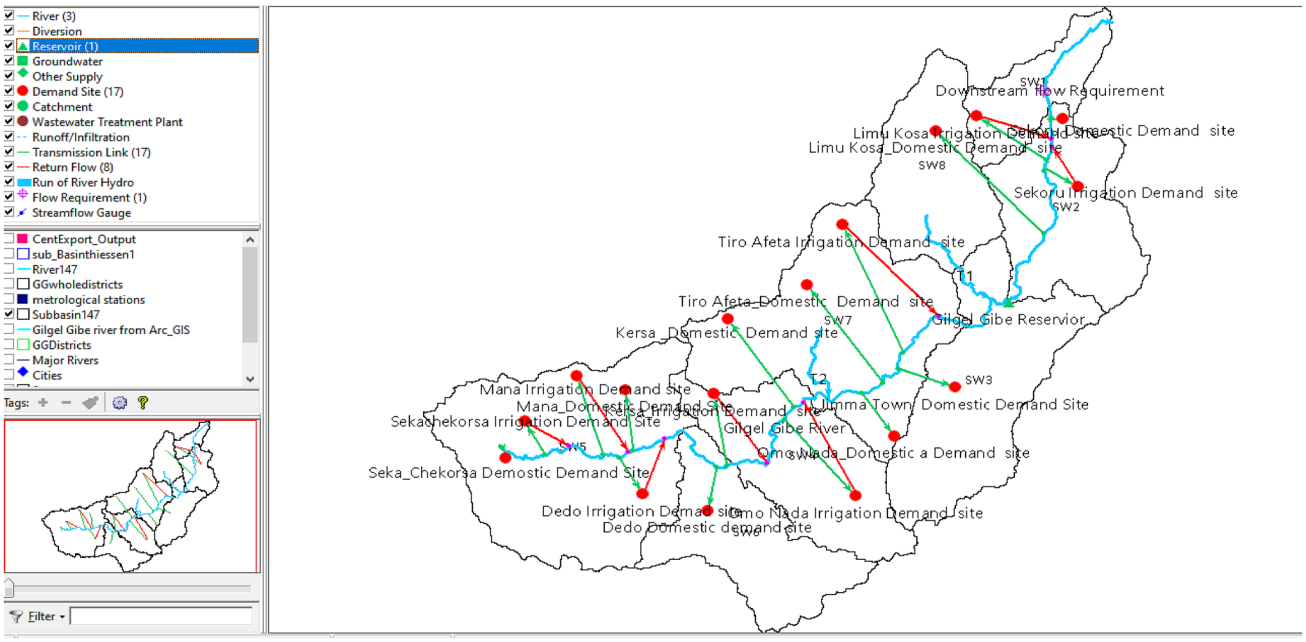

Fig. 4 Schematics of WEAP model configuration for Gilgel Gibe watershed

Scenario development in WEAP

Scenarios are self-consistent storylines that show the future trend's response under a particular socio-economic policy (Gedefaw et al. 2019). The possible future events will be projected and analyzed in scenario analysis by considering different possible outcomes (Arsiso et al. 2017; Hussen et al. 2018; Olabanji et al. 2020). The future water supply and demand analysis was conducted using seven scenarios for this study.

A. Reference scenario

The reference scenario is established based on the climate change and the socio-economic data of the current account year. The year 2019 was the current account year. The reference scenario was used as a point of comparison for all other scenarios. The current account year's projected water demand and the forecasted water supply were compared with alternative scenarios.

B. Expected population growth (EPG) and high population growth (HPG) scenario

EPG scenario is developed based on the varying growth rate of the population for the urban and rural populations. Ethiopia has the second-highest population in Africa and the 12th most populated globally. There is no obligatory population controlling policy in the country. Healthy professionals highly recommend family planning in governmental and non-governmental health institutes. However, there is no education regarding family planning mechanisms for the community. A study investigated by UNDP (2014) for over-8 successive years indicated that the population growth rate of the Gilgel Gibe watershed showed an increasing trend. Therefore, the HPG scenario was developed based on the expansion of urbanization and unlimited population increment of the watershed. The future growth rate for the study period was estimated based on the past growth rate of the population. According to OWWDSE (2010), the urban population growth rate of the Oromiya region at the end of 2000, 2005, and 2010 was 5.29, 4.88, and 4.74%, respectively. Based on this, the future urban growth rate was projected at a 10-year interval. Table 6 shows the projected urban and rural growth rates for EPG and HPG scenarios.

Table 6 Projected population growth rate

	Year			
	2019/2020	2030	2040	2050
Growth rate				
EGR (%)				
Rural	2	1.6	1.2	0.8
Urban	4.32	3.84	3.43	3
HGR (%)	4.7	4.4	4.1	3.8

Table 7 Projected annual water consumption rate

Description	Years			
	2020	2030	2040	2050
Total population	2,074,117	2,588,935	3,123,962	3,646,829
Adjusted total domestic water demand (m^3/day)	50,902	80,777	131,294	168,359
Total non-domestic water demand (m^3/day)	10,447	16,155	26,259	30,219
Total average daily water demand (m^3/day)	70,244	111,472	181,186	232,335
Annual maximum water demand (m^3/p/year)	14.84	18.86	25.4	27.9

C. Increase in consumption rate (ICR) scenario

The ICR scenario was developed based on the ever-increasing expansion of urbanization and high socio-economic status. The estimated water consumption rate (WCR) for the 2019/2020 year was 14.84 m^3/p/year. The future annual consumption rate (CR) at a 10-year interval was estimated for the ICR scenario based on the OWWDSE (2010) water supply design guideline. The result shows that the projected annual CR at the end of 2030, 2040, and 2050 will be 18.86, 25.4, and 27.9 m^3/p/year, respectively. Table7 shows the maximum annual water consumption rate computed based on the EPG rate.

D. Irrigation area expansion (IAE) scenario

Irrigation area expansion is considered due to the high agricultural activity of the community that lives in the watershed. According to the socio-economic profile of the district, the irrigation area has increased by 8.5% in the last 10 years. Due to this, a 10% hypothetical increment was projected every 10 years throughout the study period. The crop water demand of the current account year and the future period was used as input to the WEAP model to quantify the unmet irrigation water demand under the reference, IAE, NIT, and IAE with NIT scenarios.

E. New Irrigation Technology (NIT) scenario

Since agricultural activities use the largest water share, it is better to use NIT to maximize efficiency (Shumet and Mengistu 2016; Ayt Ougougdal et al. 2020). Currently, irrigation activity is mainly practiced traditionally. Drip and sprinkler irrigation are part of NIT that saves from 60 to 70% of the annual irrigation water use rate depending on the soil types, climatic condition, and crop period (Sun et al. 2018; Gedefaw et al. 2019).

F. Irrigation area expansion with NIT scenario

The combined effect of irrigation area expansion with a New Irrigation Technology (NIT) scenario was developed to identify how this scenario affects the spatiotemporal dynamic of unmet water demand compared to the increase in irrigation area expansion and the reference scenario.

Trend analysis of annual unmet domestic and irrigation water demand

Man–Kendall (MK), Sen's slope estimator (SSE), and modified Man–Kendall (MMK) tests are non-parametric statistical techniques that are widely used for trend analysis of time-series data. The methods do not require the sample to be normally distributed (Alifujiang et al. 2020). However, the MK test may overestimate the significant trend of serially correlated time-series data (Das et al. 2021). In the MMK test, it is possible to remove significant autocorrelations from the sample using different empirical equations and approaches based on the type of autocorrelation (Hamed 2009). However, the removal of significant autocorrelation may also remove significant trends. The SSE also computes the trend of time-series data using the sample's median, which excludes the contribution of lower and higher outlier data (Alashan 2020). Therefore, to overcome the drawbacks of MK, MMK, and SSE, Sen (2012) developed the innovative trends analysis (ITA) technique for trend analysis of time -series data. The method is not affected by sample size, distribution, and autocorrelation. Furthermore, the result of ITA can be easily presented and interpreted graphically. Therefore, the ITA was selected to analyze the trend of unmet demand under the different scenarios considered in this study. An innovative trend analysis and time-series change point analysis (trendchange) package was used in R-studio to conduct ITA of annual unmet domestic and irrigation water demand.

In the ITA method, the sample is divided into two equal parts. Then, scattered plots are drawn on the x–y coordinate system with the first half of the time-series data on the x-axis and the second half of the time-series data on the y-axis. Then, the trendless line is drawn at 45° on the x–y coordinate system. The trendless line divided the rectangular plane into equal parts of an upper and lower triangle. The direction of the trend (increasing/decreasing) will be based on the position of the scattered data. If the scattered plot is found on the lower triangles, the series shows a decreasing trend, whereas if the scatter plot is positioned on the upper triangle, the series shows an increasing trend. On the other hand, the series shows no trend if the scattered plot exactly

fits the trendless line. According to Machiwal et al. (2019), the trend slope of the series (S_{ITA}) is computed using Eq. (7)

$$S_{ITA} = 2\frac{(\bar{x} - \bar{y})}{n}, \tag{7}$$

where n represents the total number of the sample; $\bar{x}$ and $\bar{y}$ are the mean values of the first and second half of the series, respectively. Transforming the series into a normal probability distribution function (mean of zero and standard deviation of (σs), the confidence limit (CL) of the trend slope can be computed by Eq. (8) (Alashan 2020; Das et al. 2021);

$$\mathrm{CL}(1-\alpha) = 0 \pm \mathrm{scri}\sigma s, \tag{8}$$

where

$$\sigma s = \frac{2\sqrt{2}}{n\sqrt{n}}\sigma\sqrt{1-\rho\overline{xy}}, \tag{9}$$

where CL is the confidence limit; scri is the critical value of slope; σs is the standard deviation of the trend; σ is the standard deviation of the main series; $\rho\overline{xy}$ is the cross-correlation coefficient of the first and second half of the series.

Results and discussion

The optimum values of sensitive sub-watershed parameters

The response of parameter variation on the magnitude of runoff was measured using NSE, one of the in-built objective functions in the HEC-HMS model. The parameter change after successive optimization trials is shown in tabular form. However, the effect of parameter adjustment on the simulated runoff is measured by NSE. Based on the selected loss, transform, and routing methods, curve number, constant rate of infiltration, lag time, wave travel time, and initial abstraction were the most sensitive parameters.

In HEC-HMS, parameter adjustment is conducted using a user-specified scale factor. This study modified the initial value of CN, lag time, and initial abstraction at a 5% scale factor. The scale factor was used to adjust the initial parameters' value at each optimization trial. For example, adjusting parameter value using the ± 5% scale factor implies that 5% is added or subtracted from the parameter's initial value. The modified parameter values were used for each consecutive optimization trial. Hence, the initial values of CN, lag time, and initial abstraction were altered from − 30 to 15% from the initial values of the parameters. In this range, the NSE value varied between − 0.35 and 0.751. The loss rate parameter for the initial and constant loss was the second sensitive parameter. This parameter measures the water-holding capacity of the soil, which depends on the hydraulic conductivity of soil texture (Gebre 2015). The constant loss rate was calibrated for all sub-watersheds from the initially assumed value of 1.5 mm/h. As a result, the NSE values varied from 0.289 to 0.749. The maximum value of NSE was obtained at a scale factor of 3.65. This implies that the optimum value of constant infiltration rate of the Gilgel Gibe watershed was 5.475 mm/h during the calibration period.

The lag time is the third sensitive parameter. Initially, it was computed from the initial curve number value, the river's longest flow path, and basin slope. Even though relatively better resolution DEM was used for basin model preparation, it does not represent the accurate spatial value of the watershed parameter. Consequently, lag time also became a sensitive parameter. The optimum lag-time value was obtained at a − 20% scale factor based on the sensitivity analysis result. The initially computed value of Muskingum K was also manually varied during the model calibration phase to obtain its optimum value. Based on the result, the maximum value of Muskingum K was 70 h. The initial abstraction is the fourth sensitive parameter computed from the optimum value of CN. Similarly, the optimum value was computed by various optimization trials. Finally, the optimum value of initial abstraction for each sub-watershed was reduced by 13% from the initial value. Table 8 shows the initial and optimum values of the sub-watershed sensitive

Table 8 Initial and optimum values of sensitive parameters

Subwatershed	CN		Ia (mm)		Lag time (min)		Loss rate (mm/h)	
	Initial	Optimum	Initial	Optimum	Initial	Optimum	Initial	Optimum
SW1	83	71	10.40	21.2	83.53	66.82	1.5	5.4
SW2	82	70	11.15	22.1	117.33	93.87	1.5	5.4
SW3	85	73	8.75	19.3	170.87	136.70	1.5	5.4
SW4	85	73	8.63	19.1	118.94	95.15	1.5	5.4
SW5	84	72	9.54	20.2	133.69	106.95	1.5	5.4
SW6	85	73	8.75	19.3	96.42	77.14	1.5	5.4
SW7	83	71	10.10	20.8	142.95	114.36	1.5	5.4
SW8	81	69	11.70	22.7	123.60	98.88	1.5	5.4

Table 9 Statistical tests of error functions during the HEC-HMS model calibration and validation phases

Statistical Index	Calibration	Validation
NSE	0.75	0.72
Pbias (%)	2.3	−3.5
RSR	0.63	0.55
R^2	0.84	0.81
MAE (m^3/s)	1.344	1.63

parameters. The optimum value of curve number, lag time, and initial abstraction were reduced by 15, 20, and 13%, respectively.

During the model calibration period, the simulated and observed runoff values were compared using five types of the statistical index of agreement shown in Table 9. From the available 22 years of daily stream flow data, 15 years (1985–1999) and 6 years (2000–2005) were used for model calibration and validation, respectively. Table 9 shows the values of statistical tests of error functions during the model calibration and validation phases.

Based on Moriasi et al. (2007), Verma et al. (2010), Golmohammadi et al. (2014), Kumarasamy and Belmont (2018), if NSE > 0.65, Pbias of < 10%, $R^2 > 0.5$ RSR < 0.6, hydrological model performance is acceptable for runoff simulation. Therefore, the HEC-HMS model has an acceptable level of accuracy. Hence, it can be used for future runoff simulations of the Gilgel Gibe watershed. Figure 5a, b also shows the daily simulated and observed runoff hydrographs. The figures show similar temporal variation, which indicates the agreement of the two hydrographs during calibration and validation phases.

Gilgel Gibe watershed showed a rapid LU/LC change during the study period which causes a significant effect on the infiltration and surface runoff generation of the watershed. The densely populated forest has been cleared and converted into agricultural and grassland areas. Forest areas have more infiltration capacity and less surface runoff. However, agricultural and grassland areas have less infiltration capacity and more surface runoff than forest cover. Therefore, most of the time, the runoff value was underestimated during the calibration phase and overestimated during the validation phase. The underestimation and overestimation of

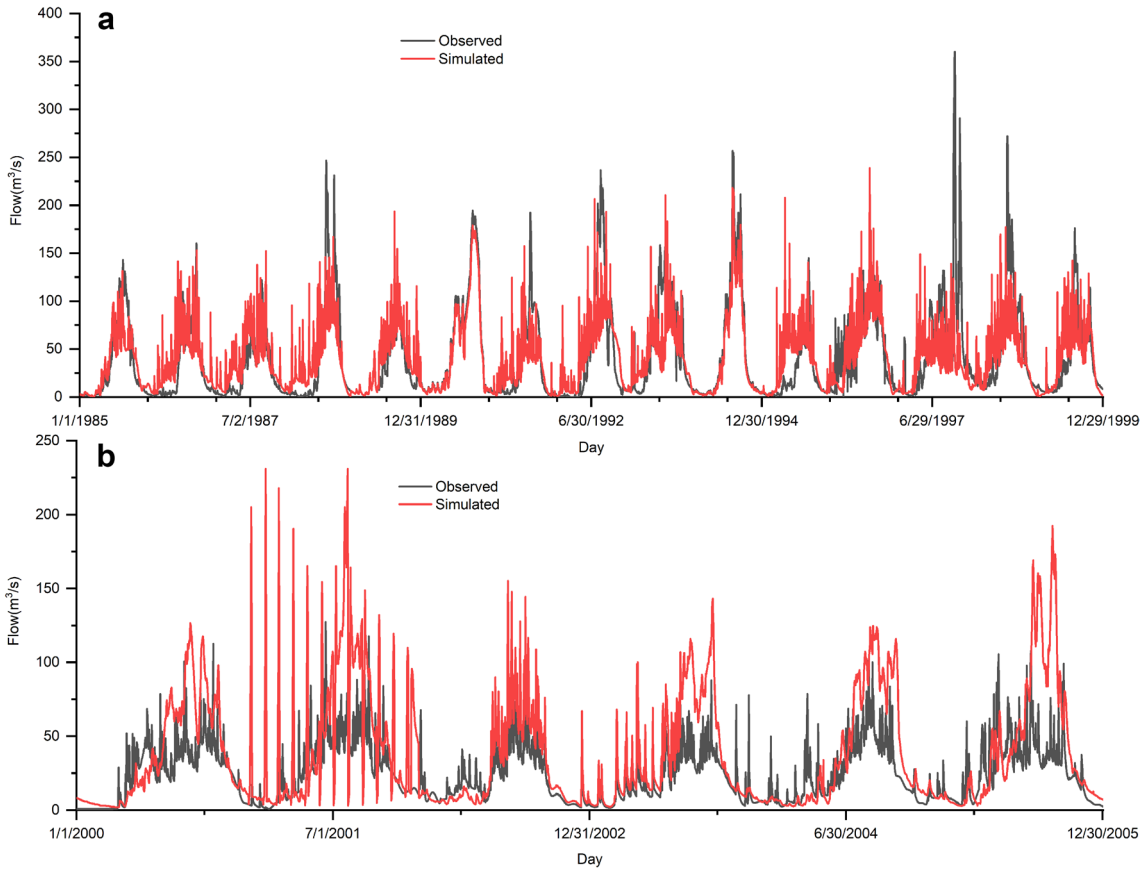

Fig. 5 The simulated and observed runoff hydrograph during model calibration and validation periods (**a** calibration phase and **b** validation phase)

Table 10 Statistical tests of error functions for runoff simulated by the RCMs output

Statistical Index	CCLM4	HIRHAM5	RACMO22T
NSE	0.65	0.58	0.63
Pbias	3.22	3.26	3.24
RSR	0.47	0.52	0.49
R^2	0.73	0.68	0.72
MAE	2.48	2.55	2.33

peak discharge during the calibration and validation phases, respectively, also showed the transformation of LU/LC from forest to the agricultural area. Takala et al. (2016) also stated that the surface runoff of the Gilgel Gibe watershed showed a decreasing trend from 1987 to 2001 and an increasing trend from 2002 to 2010.

In addition to the temporal variation of LU/LC, the significant variation between the simulated and observed runoff value was caused by the following major limitations of the SCS-CN method. (1) The method does not consider the variation of rainfall intensity with duration (Halwatura and Najim 2013). It assumes constant rainfall intensity for a fixed rainfall depth with short and long duration. (2) The SCS-CN method is developed for small agricultural areas of the mid-western temperate region. Hence, application of the method in tropical region may cause a substantial deviation between the simulated and observed runoff values (Descheemaeker et al. 2008). (3) The watershed transmission loss at the confluence between junctions of sub-watershed and reach is not accounted for by the SCS-CN method (Najim et al. 2006). Therefore, the HEC-HMS model tends to cause a significant error in the peak discharge for large watersheds. In this study, the observed peak discharge during the calibration phase was overpredicted by 2.3%. However, it was underpredicted by 3.5% during the validation phase.

Runoff simulation using RCMs' output

The precipitation outputs of CCLM4, HIRHAM5, and RACMO22T models were used to forecast the Gilgel Gibe watershed runoff. The analysis showed that the simulated stream flow of all the three RCMs was underestimated. Therefore, the use of ensemble projection will underestimate the

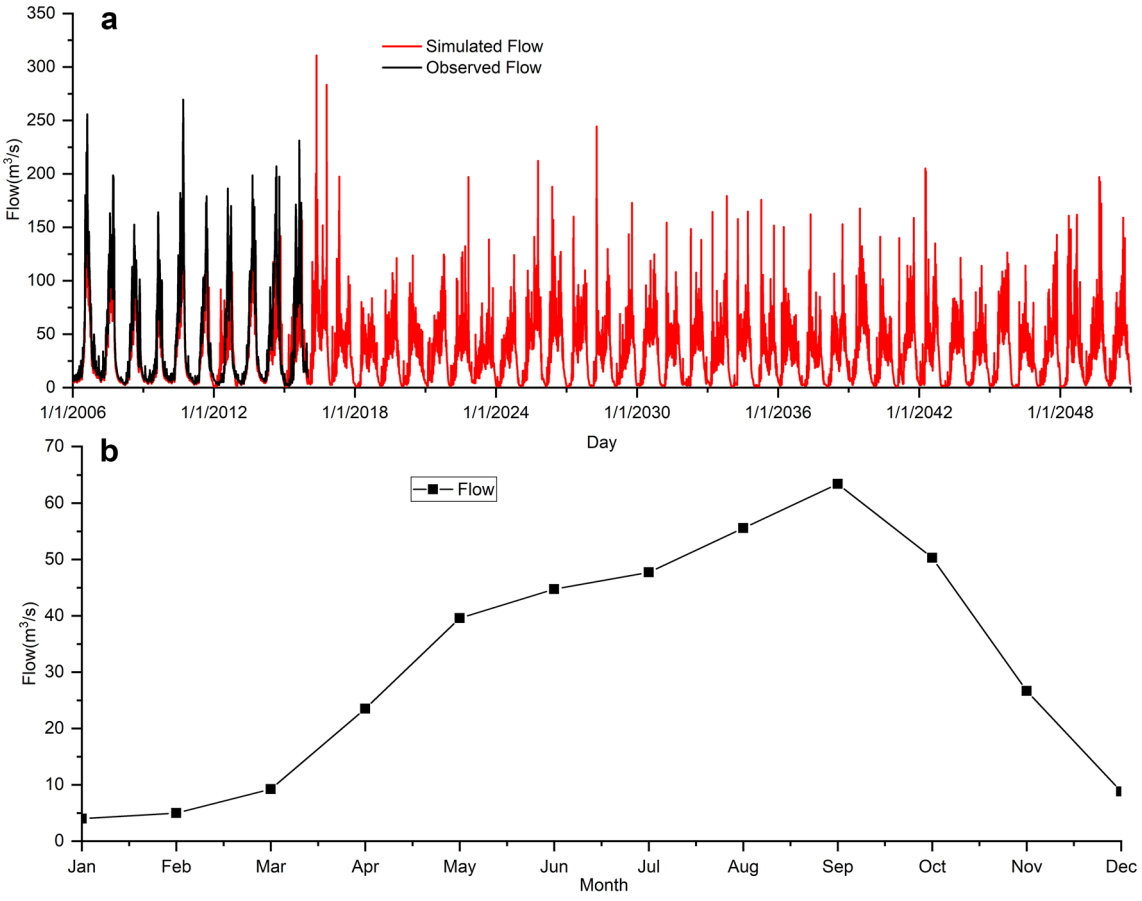

Fig. 6 The simulated (2006–2050) and observed (from 2006–2015) runoff hydrograph and monthly average stream flow (**a** simulated and observed runoff hydrograph and **b** monthly average stream flow)

stream flow of the Gilgel Gibe River. Hence, the daily simulated runoff values of each RCM were compared with the observed runoff value from 2006 to 2015 to select the most accurate RCM model. The three models' performance was measured by the same statistical test of error function used for model calibration and validation phases. The analysis showed that the CCLM4 model has more acceptable values of NSE, Pbias, RSR, R^2, and MAE (0.65, 3.22%, 0.47 m^3/s, 0.73, and 2.48), respectively. Therefore, the CCLM4 model has well predicted the future stream flow of the Gilgel Gibe watershed. Hence, the daily precipitation from 2007 to 2050 for the CCLM4 model was used to simulate the stream flow for the same temporal resolution.

Table 10 shows the values of the statistical index of the agreement for the three RCMs' output. Figure 6a also shows the simulated (2006–2050) and observed (2006–2015) runoff for the Gilgel Gibe watershed. The figure also shows that the simulated daily stream flow is similar to the observed runoff hydrograph. This also implies the accuracy of the CCLM4 model in estimating the precipitation of Gilgel Gibe watershed. Figure 6b shows the monthly average stream flow through the study period.

The unmet domestic water demand analysis

The domestic water demand for the reference scenario was estimated using the current account year's demand data. Based on the result, the annual unmet demand in 2019 was 1.89 BCM. During the year 2020, the annual unmet domestic demand decreased to 0.84 BCM. All domestic demand scenarios showed that the 2020-year unmet demand was reduced by 55% from the current account year. This is due to the availability of better watershed runoff capacity than the watershed runoff capacity of the year 2019. The reference scenario indicates that the annual unmet demand showed both decreasing and increasing trends based on the watershed's annual runoff capacity for the coming 3 decades. However, it has a minimum unmet demand value throughout the study period compared to other scenarios (Table 11; Fig. 7). For reference scenario, external anthropogenic activities are not considered. Therefore, the temporal variation of unmet water demand is related to the magnitude of watershed runoff related to the change in signal and magnitude of climate variation.

Figure 7 shows the average annual unmet demand variation for all domestic demand scenarios. The graphical visualization shows that the annual unmet demand variations for EPG, HPG, and ICR scenarios are close to that of the reference scenario. The reference scenario was driven by the climate change impact on Gilgel Gibe stream flow capacity. Therefore, the variation of annual unmet demand for the reference scenario was due to the variation of annual stream flow capacity throughout the study period. However, the EPG, HPG, and ICR scenarios were driven by the population growth, increment of consumption rate, and the variation of stream flow capacity. As shown in Table 11, the EPG, HPG, and ICR scenarios from 2019 to 2029 have a minor difference in annual unmet demand from the reference scenario. However, from 2030 to 2050, the HPG, ICR, and EPG scenarios showed a slight increment of annual unmet demand. Nevertheless, they showed similar temporal variations with that of the reference scenario. The result also showed that the average annual unmet domestic demand under the reference, EPG, HPG, and ICR scenarios throughout the study period was 1.633 BCM, whereas the average annual unmet domestic demand under the HPG scenario was 1.634 BCM. The result indicates that the increment of domestic water consumption and population growth at the specified growth rates caused minor annual unmet demand increment. As shown in Fig. 7, the average annual unmet demand is comparable under all the domestic demand scenarios.

The annual increment rate of annual unmet domestic and irrigation water demand was computed based on the linear increment of unmet water demand. The linear increment rate was then compared with the trend slope computed by ITA to obtain a more confidential result. Based on the analysis, the reference scenario's annual unmet demand increment was 0.0206 BCM/year, less than the increment rate of other scenarios considered in this study. This signifies that climate change's direct effect is less than the external man-made activities on the temporal variation of unmet demand. The EPG scenarios showed minimum annual unmet domestic demand with an annual increment rate of 0.0209 BCM/year from the externally driven scenarios. Hence, if there is no high population growth, the annual unmet demand will have a minimum increment rate. The result also showed that the

Table 11 Annual increment rate of unmet domestic water demand

Scenario	Annual increment (BCM/year)	Unmet domestic demand (BCM)				
		2019	2020	2030	2040	2050
Reference	0.0206	1.8903	0.8391	1.6583	1.9970	1.7019
EPG	0.0209	1.8903	0.8393	1.6609	2.0045	1.7093
HPG	0.0218	1.8903	0.8398	1.6653	2.0181	1.7400
ICR	0.0210	1.8903	0.8393	1.6608	2.0068	1.7125

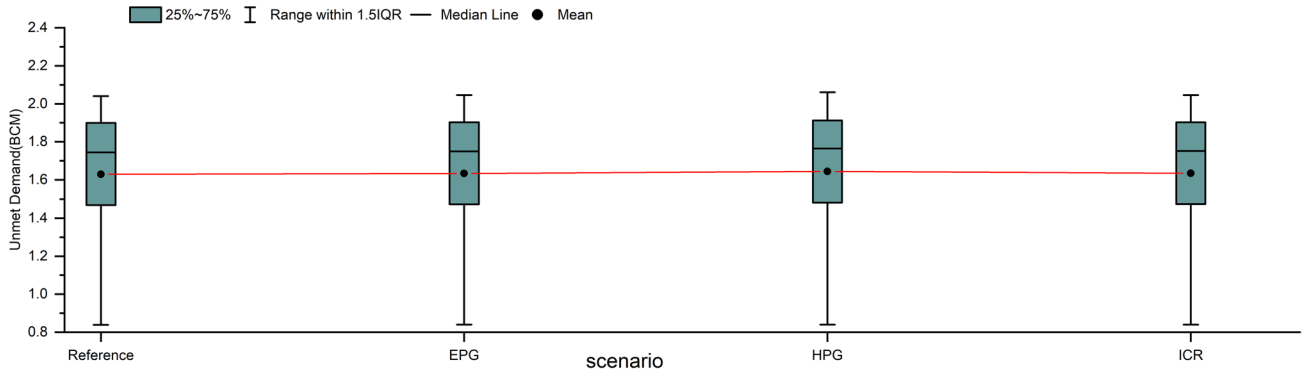

Fig. 7 The average increment of annual unmet domestic water demand

Table 12 The trend of annual domestic unmet demand

Scenario	$S_{ITA(BCM/year)}$	Scri at $\alpha = \pm 10\%$	Scri at $\alpha = \pm 5\%$
Reference	0.0165	0.0029	0.0035
EPG	0.0168	0.0029	0.0035
HPG	0.0177	0.0031	0.0037
ICR	0.0169	0.0029	0.0035

ICR scenario has a negligible difference in increment rate from the EPG scenario (0.021 BCM/year). The result indicates that consumption rate increment on unmet domestic demand was minimal compared to population growth scenarios. The finding is also proved by Psomas et al. (2017), Alemu and Dioha (2020), Ayt Ougougdal et al. (2020), Yao et al. (2021). Hence, population growth is the main driving factor for the increased unmet demand. On the other hand, the HPG scenario has the highest annual increment rate (0.0218 BCM/year). This indicates that the annual unmet demand under the HPG scenario shows a faster increment than in other scenarios. However, the variation in annual unmet demand under the EPG, HPG, and ICR from the reference scenario was gradual (Table 11). This finding also agrees with the study of Mourad and Alshihabi (2016), Hussen et al. (2018), Al-Mukhtar and Al-Yaseen (2019a; b), Alemu and Dioha (2020). The result also showed that the maximum annual unmet demand was 2.05 BCM for reference and EPG scenarios. Under the HPG scenario, the maximum annual unmet demand was 2.06 BCM. However, the maximum unmet demand for all scenarios, except the HPG scenario, was observed in the year 2034. However, the maximum observed HPG scenario was in the year 2040.

The trend of annual unmet demand was analyzed using ITA to quantify the significance of the decreasing rate of annual unmet domestic and irrigation demand. The analysis was also used to compare the result of the linear increment rate. As shown in Table 12, the S_{ITA} value of annual unmet domestic demand under the reference, EPG, HPG, and ICR scenarios showed an increasing trend. The significance of the annual unmet demand increment was evaluated at 5 and 10% significance levels. Based on the result, the S_{ITA} value was greater than the Scri value at the specified significance levels for all domestic water demand scenarios. Hence, all scenarios showed significant annual unmet domestic demand increment throughout the study period. The ITA result also showed that the annual unmet demand for the reference and HPG showed the minimum and maximum significant increasing trend.

The annual unmet demand from 2019 to 2050 was divided into two equal parts. The scattered plot of the first half of the series (2019–2034) was drawn on the *x*-axis, whereas the scattered plot of the second half of the series (2035–2050) was drawn on the *y*-axis. As shown in Fig. 8, in the scattered plot of the annual unmet domestic demand under the reference, EPG and HPG were positioned above the trendless line (on the upper triangle). This indicates that the trend was significant throughout the study period. However, the difference in annual unmet domestic water demand between scenarios is not noticeable. Figure 8 shows the ITA result of annual unmet demand under the reference and HPG scenarios.

Spatial variation of annual unmet domestic water demand

It is essential to show the spatial distribution of unmet demand in the watershed. A district with a high unmet demand area is a hot spot area that will require special care on the demand and supply side. In this study, all the domestic demand sites have a demand priority of one. Therefore, the unmet domestic demand distribution was based on the district's population and the relative location of the domestic demand site. At each irrigation demand site, a 5% return flow was assumed during the study period. Therefore, the return flow from the upstream irrigation demand site is assumed to return to the Gilgel Gibe River. Accordingly,

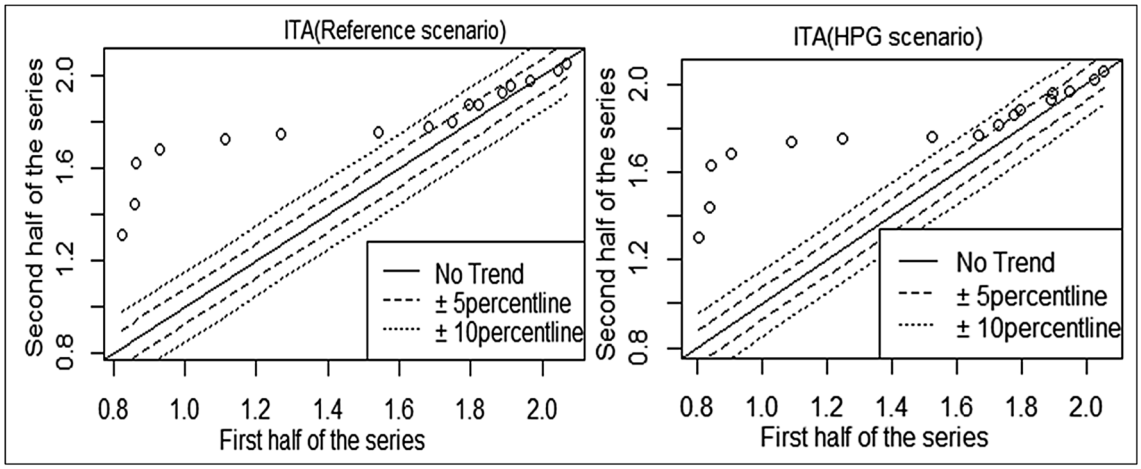

Fig. 8 Scattered plot of annual unmet domestic water demand for reference and HPG scenarios

Table 13 The total population of the Gilgel Gibe watershed under EPG rate

Census 2019		2020	2030	2040	2050	
Growth rate (%)						
Rural		2	1.6	1.2	0.8	
Urban		4.32	3.84	3.424	3	
Districts	Rural	Urban	Total	Total population		
Dedo	241,964	13,153	255,117	260,524	314,656	365,172	407,425
Limmu Kosa	204,429	45,624	250,053	256,113	320,338	387,442	453,464
Manna	188,051	18,400	206,451	211,007	257,459	302,506	342,530
Omo Nada	197,709	21,069	218,778	223,642	273,404	321,985	365,579
Kersa	223,225	9359	232,584	237,453	285,905	330,544	367,087
Seka Chekorsa	280,581	12,124	292,705	298,840	359,936	416,299	462,548
Sokorru	172,473	21,946	194,419	198,817	244,137	289,041	330,205
Tiro Afeta	163,253	9157	172,410	176,071	212,745	247,028	275,784
Jimma town		202,886	202,886	211,651	320,355	463,944	642,207
Total	1,671,685	353,718	2,025,403	2,074,117	2,588,935	3,123,962	3,646,829

Table 14 The total population of the Gilgel Gibe watershed under HPG rate

Year	2019	2020	2030	2040	2050
District	Census	(4.7% GR)	(4.4% GR)	(4.1% GR)	(3.8% GR)
Dedo	255,117	267,107	429,169	667,708	1,037,140
Limmu Kosa	250,053	261,805	421,233	655,361	1,013,757
Manna	206,451	216,154	347,439	540,551	838,633
Omo Nada	218,778	229,061	368,212	572,870	888,573
Kersa	232,584	243,515	391,216	608,660	945,760
Seka Chekorsa	292,705	306,462	492,349	766,003	1,190,202
Sekoru	194,419	203,557	327,273	509,176	789,363
Tiro Afeta	172,410	180,513	290,041	451,250	700,884
Jimma town	202,886	212,422	344,729	536,335	808,364
Total population	2,025,403	2,120,597	3,411,661	5,307,914	8,212,675

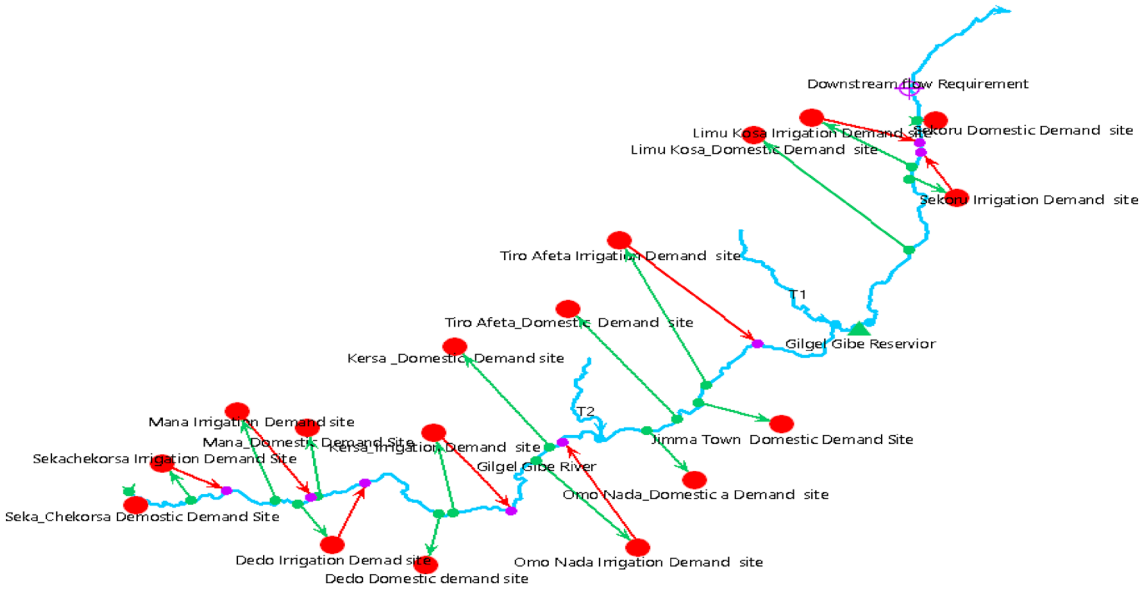

Fig. 9 The relative location of demand site in Gilgel Gibe watershed

the downstream demand site can withdraw the return flow. Tables 13 and 14 show the projected population for the current account year and 2020 to 2050 at 10-year intervals under EPG and HPG scenarios.

Considering the relative location of domestic demand sites, the Seke_Chekorsa district is the upstream demand site (Fig. 9). However, the downstream most demand site is Sekoru. Seka_chekorsa district also has the highest population under EPG and HPG scenarios. Therefore, the maximum unmet demand was shown on the Seka_Chekorsa domestic demand site, and the minimum unmet demand on the Sekoru domestic demand site. As shown in Figs. 10 and 11, except for the HPG scenario, the Sekoru domestic site showed demand coverage of 100% for all scenarios for the 2019–2050 periods. However, the study period showed minimum unmet demand under the HPG scenario. Therefore, the Seka_Chekorsa district showed the highest water supply scarcity, indicating the necessity of alternative water supply sources.

The unmet irrigation water demand analysis

The unmet irrigation water demand was computed based on the reference, IAE, IAE with NIT, and NIT scenarios. During the reference scenario, the irrigation area of the current account year was directly projected for the future period. However, the annual crop water consumption rate increment due to climate change was considered under the reference scenario. Based on the analysis, the IAE scenario showed that the annual unmet water for irrigation was 1.89 BCM during the current account year. This reduced to 1.275 BCM in the year 2020. However, it showed a 34% increment from the reference scenario during the year 2020. The annual unmet demand fluctuated based on the water resource of the Gilgel Gibe watershed. The analysis indicates that the IAE showed an annual increment rate of 0.09 BCM/year throughout the study period, the maximum increment from the irrigation scenarios. The result also showed that the minimum and maximum annual unmet irrigation water demand were 1.28 BCM and 4.44 BCM during the years 2020 and 2050, respectively. In the year 2050, the IAE scenario showed a 68% increment from the reference scenario, which is double-fold compared to the increment rate of 2020. Different researchers from the different watersheds of Ethiopia. Adgolign et al. (2016); Shumet and Mengistu (2016); Gedefaw et al. (2019) also proved that high unmet demand would be obtained from irrigation area expansion scenario.

Under IAE with NIT scenario, the average annual unmet demand was reduced by 59 and 77.4% from the annual unmet water demand of the reference and IAE scenarios. At the same time, the maximum annual unmet demand showed a reduction of 57 and 7.35% from the IAE and reference scenarios, respectively. As a result, the annual increment rate of unmet demand under IAE is greater than fourfold from the irrigation IAE with NIT scenario (0.022 BCM/year). The NIT scenario showed a decline rate of −0.0003 BCM/year. This indicates that the annual unmet demand of this scenario was less than all the irrigation scenarios throughout the study period. Sun et al. (2018) and Ayt Ougougdal et al. (2020) also proved that minimum annual unmet demand can be obtained from the NIT scenario. The result signifies that the NIT scenario without irrigation expansion showed fewer

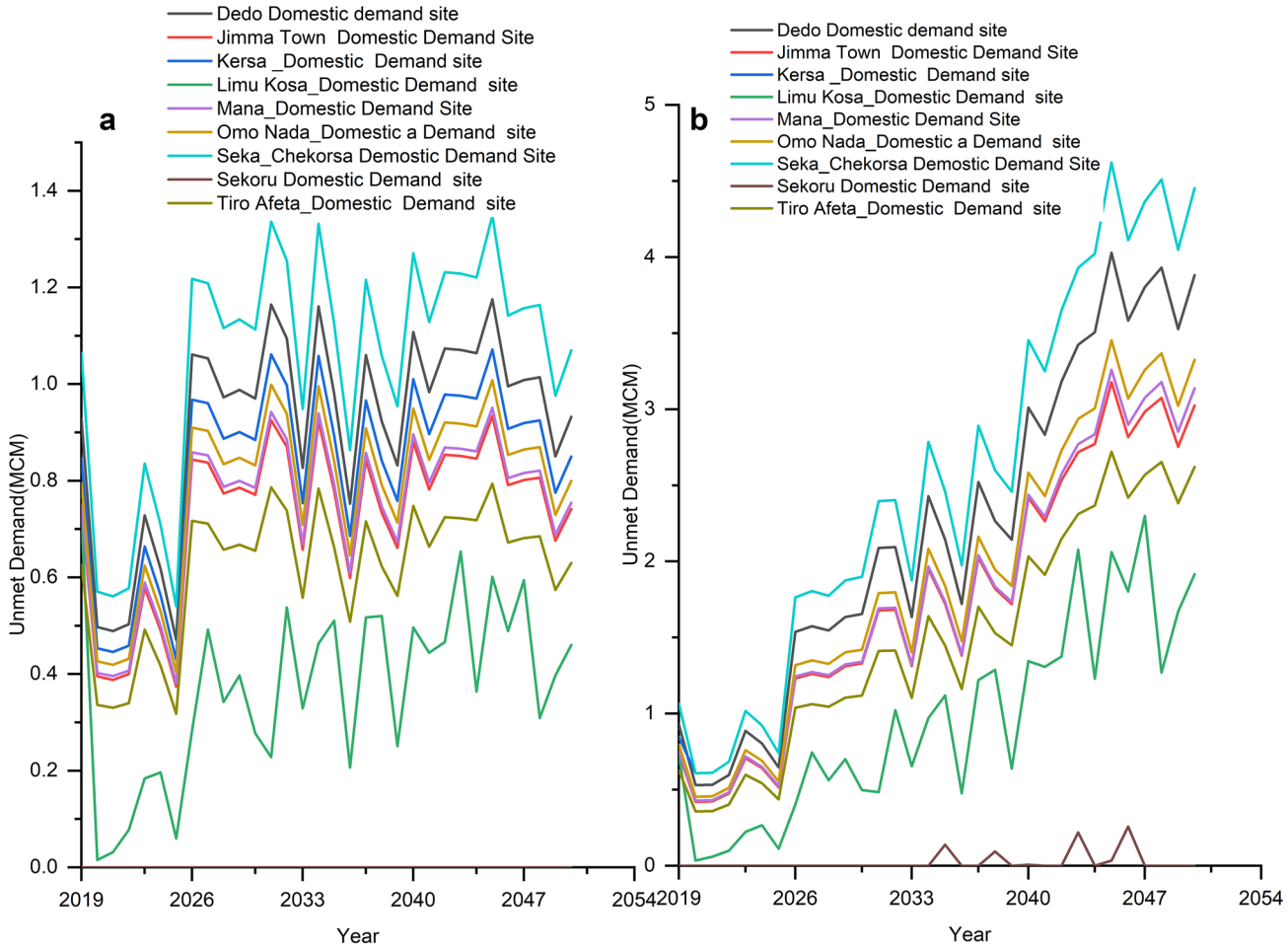

Fig. 10 Spatiotemporal variation of annual unmet demand under reference and HGR scenarios (**a** reference scenario and **b** HGR scenario)

water scarcity problems. NITs such as drip and sprinkler irrigation can save a minimum of 70% of irrigation water by reducing loss and maximizing overall water application efficiency. This indicates that the future agricultural activity will be more efficient than the existing irrigation practice with the NIT scenario.

All domestic and irrigation scenarios showed that the unmet demand could not be avoided. Alemu and Dioha (2020) have stated that none of the domestic scenarios satisfied Addis Abeba city's unmet water demand. Therefore, agricultural expansion without any future water availability consideration may cause water scarcity and conflict of interest between the upstream and downstream users. This can be minimized using the NIT scenario for the long-term plan.

The mountainous topography of the area, availability of groundwater at shallow depth, and coffee and large fruits production are good opportunities to transform the traditional irrigation system into a new drip and sprinkler irrigation system, whereas for a short-term plan shifting cropping pattern, as stated by Mourad and Alshihabi (2016), and Silva et al. (2020), use of groundwater using simple technology such as hand-dug well and Polly system, rainwater harvesting, and water loss minimization in the distribution system are highly recommended to maximize the available water resource of Gilgel Gibe watershed (Table 15).

To quantify the significance of the increment, the trend of annual unmet irrigation water demand was also investigated using ITA. Based on the analysis, the maximum S_{ITA} value of unmet irrigation water demand was for the IAE scenario ($S_{ITA}=0.0787$ BCM/year). This signifies that the increment in annual unmet demand under IAE is the highest compared with the other scenarios' annual unmet demand. However, the IAE with NIT scenario showed a higher increment in annual unmet demand ($S_{ITA}=0.0145$ BCM/year), than that of the reference scenario ($S_{ITA}=0.0166$ BCM/year). In contrast, under NIT scenarios, annual unmet irrigation water unmet demand showed a decreasing trend ($S_{ITA}=-0.0016$ BCM/year). On the other hand, the S_{ITA} value of annual unmet irrigation water demand under the NIT scenario at 5 and 10% significance levels is less than the Scri value

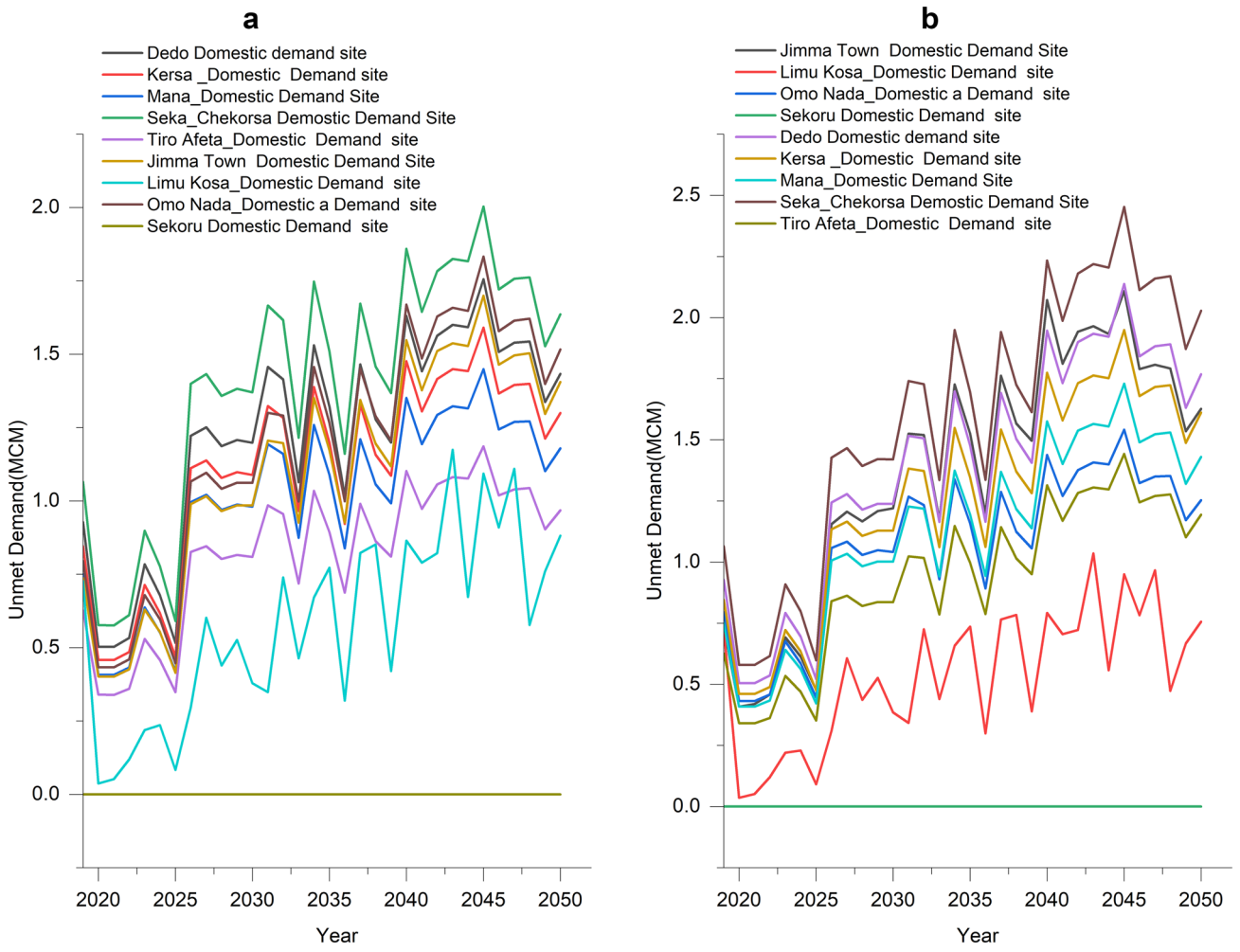

Fig. 11 Spatiotemporal variation of annual unmet water demand under ICR and EPG scenarios (**a** ICR scenario and **b** EPG scenario)

Table 15 Summary of unmet irrigation water demand

Scenario	Increment (BCM/year)	Minimum (BCM)	Year	Unmet water demand							
				Maximum (BCM)	Year	Average (BCM)	2019	2020	2030	2040	2050
Reference	0.0206	0.80	2025	2.04	2034	1.63	1.89	0.07	0.34	0.41	0.23
IAE	0.09	1.28	2020	4.44	2050	2.97	1.89	1.28	2.74	3.46	4.44
IAE with NIT	0.022	0.08	2025	1.89	2019	0.67	1.89	0.84	1.66	2	1.7
NIT	−0.0003	0.02	2025	1.89	2019	0.35	1.89	0.13	0.64	0.77	1.04

(Table 16). This indicates that the decreasing rate was not significant.

The scattered plot of annual unmet demand for IAE, IAE with NIT, and NIT is plotted in Fig. 12. The scattered plots of annual unmet demand for the IAE and IAE with NIT scenarios are located on the upper triangle of the *x*–*y* coordinate system. The scattered plots of annual unmet irrigation

Table 16 The trend of annual irrigation unmet water demand

Scenarios	S_{ITA} (BMC/year)	$\alpha = \pm 10\%$	$\alpha = \pm 5\%$
Reference	0.0166	0.0029	0.0035
IAE	0.0787	0.0041	0.0049
IAE with NIT	0.0145	0.0038	0.0046
NIT	−0.0016	−0.0049	−0.0058

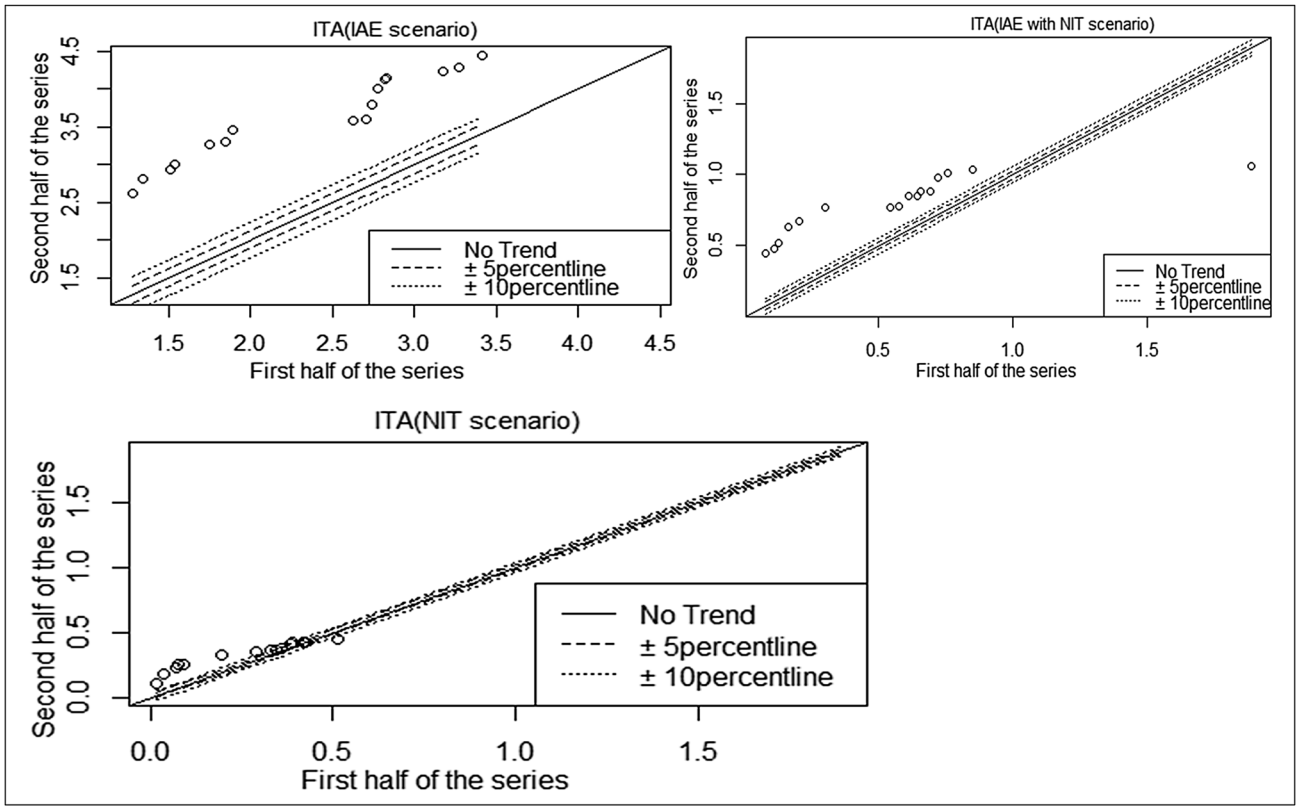

Fig. 12 Scattered plot of annual unmet demand under irrigation scenarios

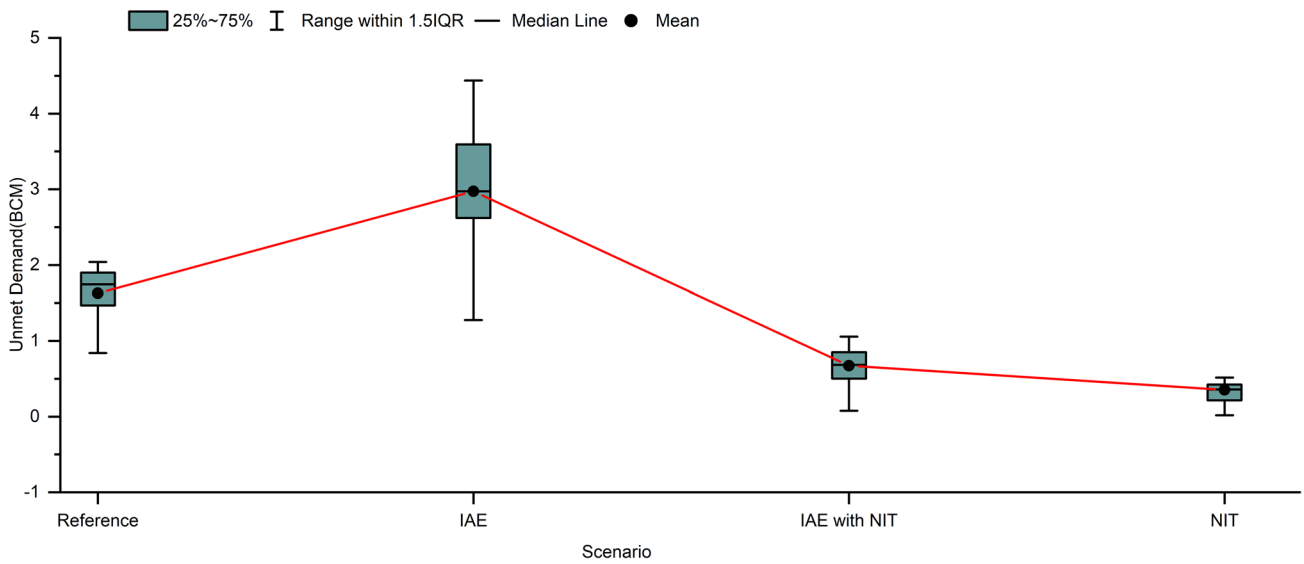

Fig. 13 The average annual unmet water demand variation under irrigation scenarios

water demand also have the maximum distance from the trendless line. Hence, the result showed a consistent and maximum increasing trend. On the other hand, the scattered plots of annual unmet demand under NIT scenarios are close to the trendless line, and they started to move toward the lower triangle. This showed that the annual unmet demand is decreasing under the NIT scenario.

Table 17 Irrigation area of each district during the study period

Year	Net irrigated area for each district (ha)							
	Dedo	Kersa	Limu_Kosa	Mana	Omo Nada	Seka _Chekorsa	Sekoru	Tiro Afeta
2019	4577	5767	7761	2959	4609	2959	5027	5617
2020	5035	6344	8537	3254	5070	3254	5530	6179
2030	5950	7497	10,089	3846	5992	3846	6536	7302
2040	6203	7816	10,518	4010	6247	4010	6813	7612
2050	8034	10,122	13,622	5193	8090	5193	8824	9859

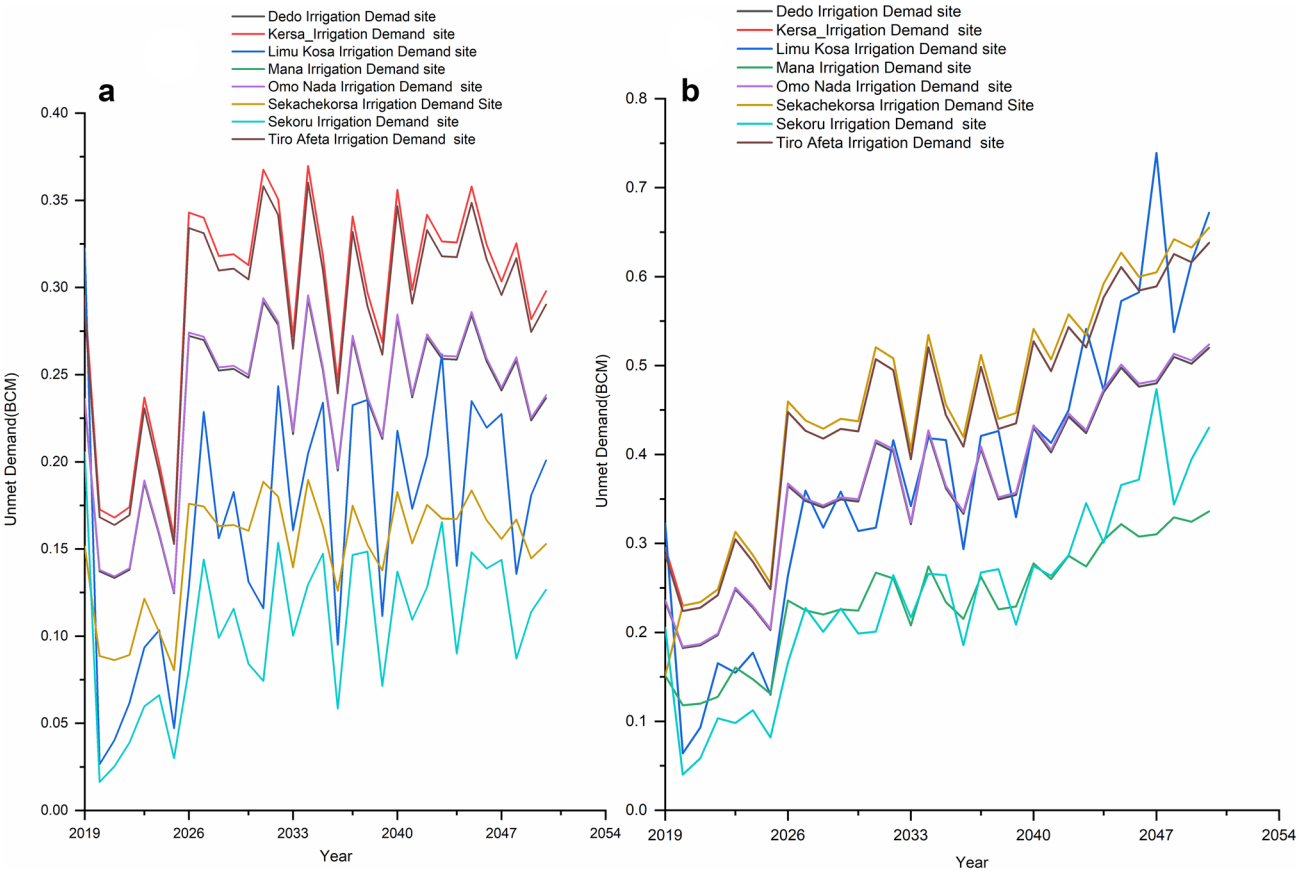

Fig. 14 Spatiotemporal dynamics of annual unmet demand for reference and IAE scenario (**a** reference scenario and **b** IAE scenario)

Figure 13 also shows the annual unmet demand box plot under the reference and irrigation demand scenarios. The figure also showed that the IAE scenarios obtain maximum annual unmet demand. However, the application of NIT in a combination of IAE scenarios can reduce the annual unmet demand.

Spatiotemporal variation of unmet irrigation water demand

In addition to temporal variation, it is important to identify the spatial variation of unmet irrigation demand sites under each irrigation scenario. This will be an input for special attention to the future water resource management scenarios. In this study, each irrigation demand site was assumed to have a demand priority of one. Therefore, the spatial variation of the unmet demand site was based on the irrigation area and location of the irrigation demand site.

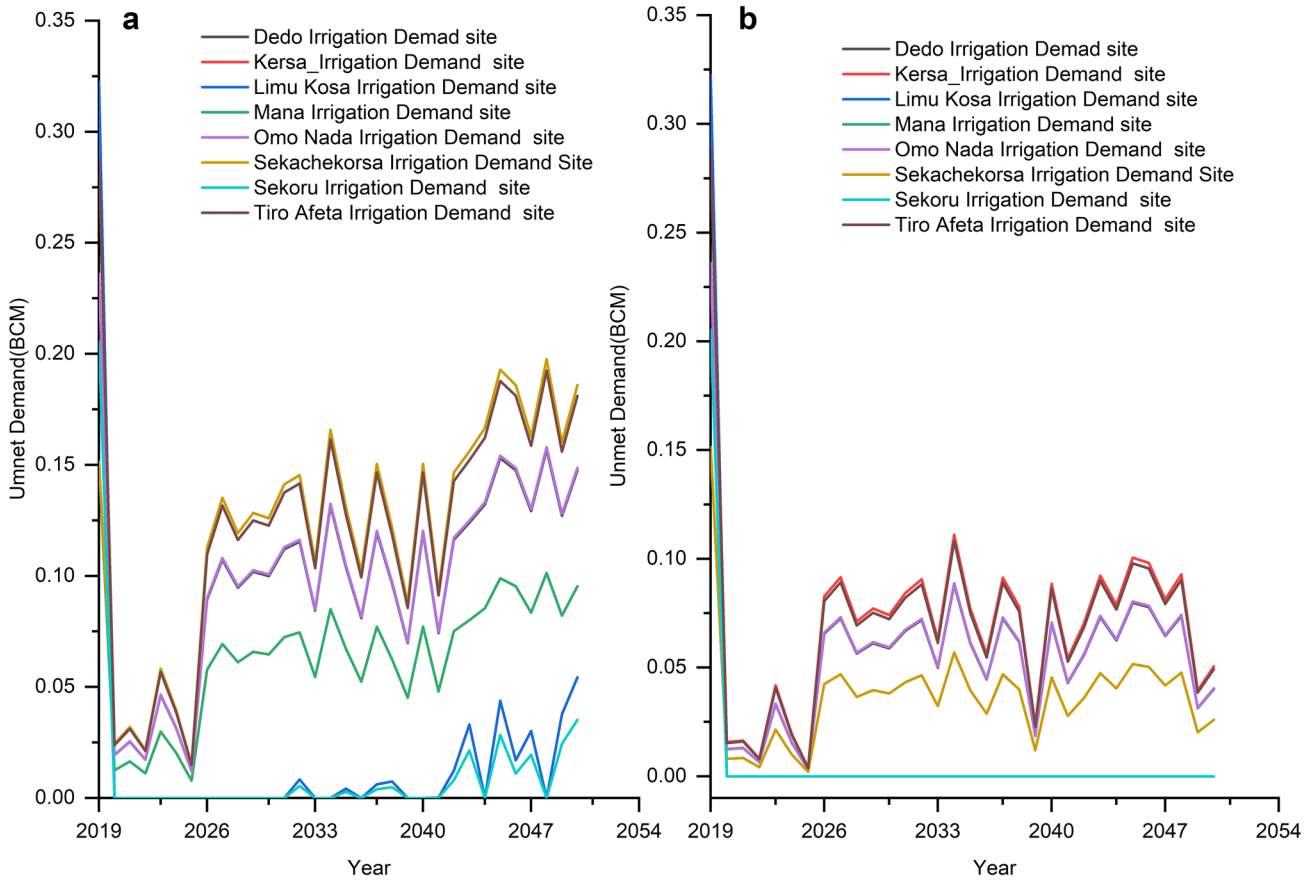

Fig. 15 Spatiotemporal dynamics of annual unmet demand for IAE with NIT and NIT scenarios (**a** IAE with NIT scenario and **b** NIT scenario)

Irrigation demand sites located immediately downstream of the domestic demand site showed a higher annual unmet demand site. Because the domestic demand site can consume the return flow released from the upstream irrigation demand site. As shown in Table 17, the Limu Kosa irrigation demand site has the highest irrigation area. However, it is located downstream of the Sekoru irrigation demand site, whereas the Kersa irrigation demand site is located downstream of Dedo domestic demand site. Therefore, Kersa and Sekoru irrigation demand sites showed the highest and lowest annual unmet demand. The remaining irrigation demand site follows a similar trend.

The effect of NIT will be more effective for the irrigation demand site with a higher irrigation area than the remaining demand site. For example, Figs. 14 and 15 for IAE with the NIT scenario show that the highest unmet demand will be for the Seka_Chekorsa irrigation demand site, whereas for the NIT scenario, this demand site is the second-lowest unmet demand site. Therefore, it should be noted that NIT technology is more effective in higher irrigation areas.

Analysis of the Gilgel Gibe I hydropower generating capacity under the domestic and irrigation water demand scenarios

The Gilgel Gibe hydropower production was also forecasted under the impact of domestic and irrigation water consumption scenarios. Since the main water source of Gilgel Gibe I hydropower is Gilgel Gibe River, alteration of water consumption policy may affect the power generating capacity. In this study, agricultural activities consumed the largest share of water. Therefore, the power production capacity is highly reduced due to agricultural activity. Based on the result, the annual power production capacity declined under all scenarios. However, the declining rate varies under different scenarios. For example, the power generation under domestic demand scenarios showed slight variation from the reference scenario (Fig. 16). The power production capacity due to the irrigation area expansion scenario reduced from 0.03 to 12% compared to the reference scenario throughout the study period. In comparison, the production capacity increased by 15.27% from the reference scenario for the NIT scenario. Therefore, better irrigation technology and water consumption habits reduce the amount of water used

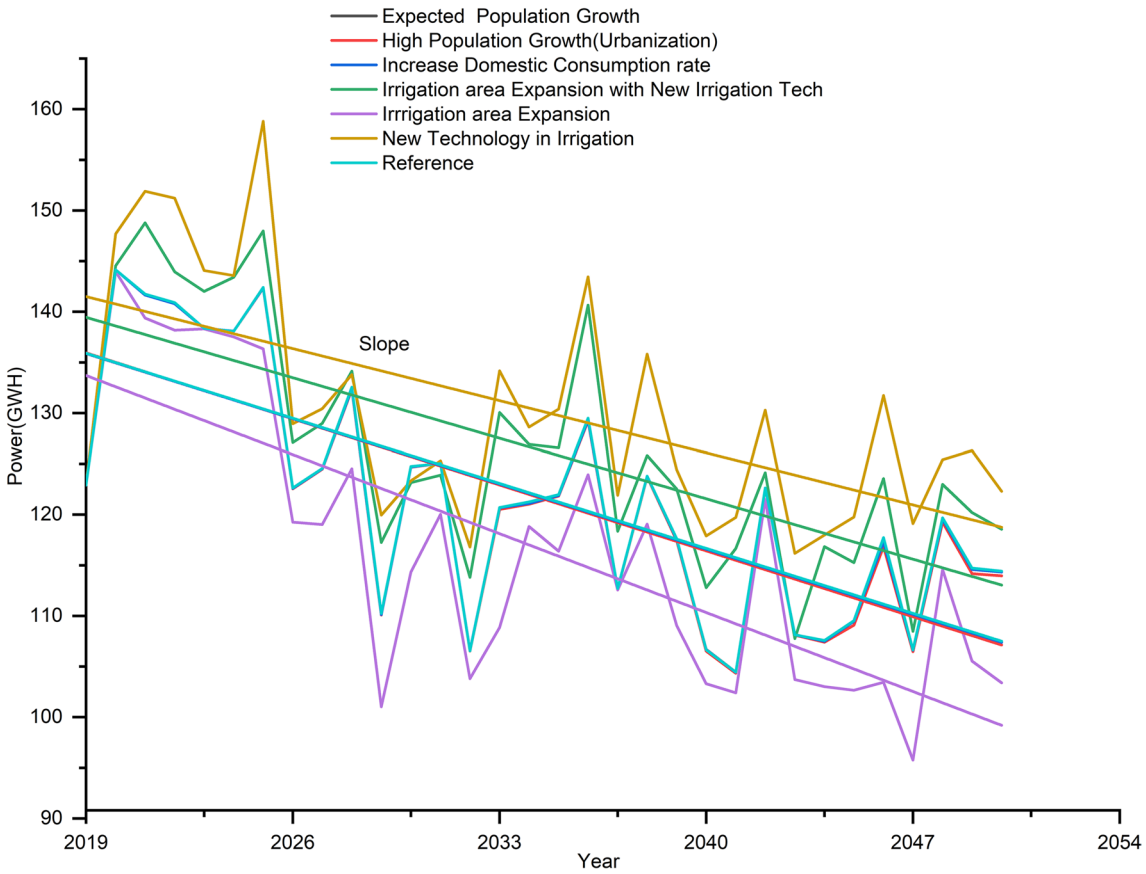

Fig. 16 Annual projected hydropower production capacity under all scenarios

Table 18 The hydropower production capacity of Gilgel Gibe I plant under the domestic and irrigation water demand scenarios

Scenario	Decline rate (GWh/year)	Power production (GWH)				
		2019	2020	2030	2040	2050
Expected population growth	−0.918	122.92	144.15	124.70	106.69	114.38
High population growth	−0.929	122.92	144.15	124.68	106.53	113.95
Increase domestic consumption rate	−0.919	122.92	144.15	124.71	106.67	114.34
Irrigation area expansion with new irrigation technology	−0.852	122.92	144.54	123.16	112.79	118.55
Irrigation area expansion	−1.113	122.92	143.97	114.33	103.30	103.40
New irrigation technology	−0.734	122.92	147.69	123.34	117.89	122.29
Reference	−0.916	122.92	144.15	124.74	106.65	114.43

for irrigation. Consequently, the power generation capacity increased under efficient and better water resource management options.

The maximum and minimum annual power production decline rates were obtained under IAE and NIT scenarios (1.113 and 0.734 GWH/year, respectively). The reference scenario showed a lower decline rate. This indicates that climate change has a lower impact on power production than anthropogenic and socio-economic activities. The return flow from the domestic demand site is insignificant. Therefore, domestic demand scenarios have a higher annual power production decline rate. Table 18 shows the declining annual rate and production capacity at 10-year interval. Based on Fig. 16, the maximum and minimum power production was obtained under IAE and NIT scenarios, respectively, throughout the study period.

Conclusion and recommendations

In this study, the unmet demand of the Gilgel Gibe watershed was assessed under the impact of climate change (as a reference scenario), EPG, HPG, ICR, IAE, IAE with NIT, and NIT scenarios. The stream flow of the Gilgel Gibe watershed was simulated using the HEC-HMS model based on the observed data set from 1999 to 2005. The model performance was measured by NSE, Pbias, RSR, R^2, and MAE. The model calibration and validation result showed that the simulated runoff well matches the observed runoff values during the calibration and validation periods. However, the HEC-HMS model better performed during the calibration period than the validation period. The significance of annual domestic and irrigation unmet water demand was investigated using the ITA. The watershed runoff was simulated by the precipitation and temperature projected by CCLM4, HIRHAM5, and RACOM22T from 2006 to 2015, and was compared with the observed runoff value. The result showed that the stream flow simulated by the CCLM4 dataset was closer to the observed stream flow with NSE, Pbias, RSR, R^2, and MAE values of 0.65, 3.22%, 0.47 m^3/s, 0.73, and 2.48, respectively. Hence, the stream flow from 2016 to 2050 was simulated using the datasets of CCLM4.

The unmet demand analysis showed that the annual increment rate of the reference scenario was 0.0206 BCM/year which is the lowest increment rate from the domestic demand scenario. In comparison, the highest increment rate was 0.02180 BCM/year under the HPG scenario. The reference, ICR, and EPG scenarios showed average annual unmet demand of 1.63 BCM through the study period. However, the average annual unmet demand for the HPG scenario was 1.64 BCM. This indicates that population is the main driving factor for water scarcity. The ITA of the annual unmet domestic water demand showed that the increment of annual unmet demand under all the domestic water demand scenarios was significant at 5 and 10% significance levels. Based on the ITA analysis, the minimum and maximum increasing trends of annual unmet domestic water demand were obtained under the reference and HPG scenarios (0.0165 and 0.0177 BCM/year, respectively).

The spatial variation of unmet demand was based on the population of the district and the relative location of domestic demand sites. The domestic demand site downstream of irrigation demand consumes the flow from the irrigation demand site. The upstream most demand site is Seka_ Chekorsa, with the highest population. In comparison, the downstream most demand site is Sekoru. Therefore, the maximum and minimum unmet water demand was for Seka Chekorsa and Sekoru domestic demand sites.

Under the irrigation scenario, the highest increment rate was for the IAE. The maximum average unmet demand was 2.97 BCM under the IAE scenario. This is also the maximum average unmet demand for all scenarios. The increment rate of IAE was 0.09 BCM/year, which is the highest increment rate from all scenarios. Under IAE with NIT scenario, the average annual unmet demand reduced by 59 and 77.4% from the reference and IAE scenarios, respectively. The minimum average annual unmet demand was 0.35 BCM. It was obtained under the NIT scenario. The result signifies that if there is no irrigation area expansion, the use of NIT will decrease the annual unmet demand by 0.0003 BCM/year. The irrigation area and relative location of the irrigation demand site govern the spatial distribution of unmet irrigation demand. Due to their location, Kersa and Sekoru irrigation demand sites have the highest and lowest annual unmet demand. The increasing trend of unmet irrigation water demand under the reference, IAE, and IAE with NIT scenario was significant, whereas the NIT scenario showed insignificant decreasing trend. The ITA result also indicates that the IAE scenarios showed the maximum increasing trend (0.0787 BCM/year), whereas the unmet irrigation water demand showed decreasing trend under NIT scenario (−0.0016 BCM/year).

The power production capacity of Gilgel Gibe I hydropower decreased under all scenarios. However, under the IAE scenario, the annual power production capacity decreased from 0.03 to 12% throughout the study period. Under irrigation area expansion and NIT scenarios, the maximum and minimum annual power decline rates were 1.113 and 0.734 GWH/year.

The finding showed that unlimited human demand is more water scarcity driving factor than climate change. Therefore, anthropogenic activities should be in line with the available water resources to minimize the water scarcity problem. Minimizing losses in water storage and conveyance system, use of water-saving irrigation technologies, rainwater harvesting, and construction of detention reservoirs to store the peak flood during the rainy season are highly recommended to minimize the unmet demand. The output of this finding is based on the likely future scenarios which may change according to the climate and socio-economic conditions. Hence, further studies should be conducted that combine the alternative water demand and best management scenarios for efficient future information of the watershed. However, the study can be used as a guideline for developing water resource management and local-scale mitigation measures.

Acknowledgements The authors would like to acknowledge the Jimma zone irrigation authority, Jimma zone plan and cooperative office, the Ministry of Water, Irrigation and Electricity of Ethiopia, and the National Metrological Agency of Ethiopia for providing the necessary data for this study. In addition, we would like to sincerely acknowledge the Stockholm Environmental Institute for providing the last updated WEAP model free of charge. Finally, we also acknowledge the two

anonymous reviewers for their valuable contribution, and strictly follow up during the reviewing stage of the manuscript.

Declarations

Conflict of interest The authors declare that they have no conflict of interest.

References

Abera Abdi D, Ayenew T (2021) Evaluation of the WEAP model in simulating subbasin hydrology in the Central Rift Valley basin, Ethiopia. Ecol Process. https://doi.org/10.1186/s13717-021-00305-5

Adgolign TB, Rao GVRS, Abbulu Y (2016) WEAP modeling of surface water resources allocation in Didessa Sub-Basin, West Ethiopia. Sustain Water Resour Manag 2(1):55–70. https://doi.org/10.1007/s40899-015-0041-4

Agarwal S, Patil JP, Goyal VC, Singh A (2019) Assessment of water supply-demand using water evaluation and planning (WEAP) model for Ur River watershed, Madhya Pradesh, India. J Inst Eng (India) Ser A 100(1):21–32

Alashan S (2020) Combination of modified Mann–Kendall method and Şen innovative trend analysis. Eng Rep 2(3):1–13. https://doi.org/10.1002/eng2.12131

Alemu ZA, Dioha MO (2020) Modelling scenarios for sustainable water supply and demand in Addis Ababa city, Ethiopia. Environ Syst Res. https://doi.org/10.1186/s40068-020-00168-3

Alifujiang Y, Abuduwaili J, Maihemuti B, Emin B, Groll M (2020) Innovative trend analysis of precipitation in the Lake Issyk-Kul Basin, Kyrgyzstan. Atmosphere 11(4):1–16. https://doi.org/10.3390/atmos11040332

Allen RG et al (2004) Revised FAO procedures for calculating evapotranspiration—irrigation and drainage paper no. 56 with testing in Idaho. Watershed Manag Oper Manag. 2000

Al-Mukhtar M, Al-Yaseen F (2019a) Modeling water quality parameters using data-driven models, a case study Abu-Ziriq marsh in south of Iraq. Hydrology 6(1):1–17. https://doi.org/10.3390/hydrology6010021

Al-Mukhtar M, Al-Yaseen F (2019b) Modeling water quality parameters using data-driven models, a case study Abu-Ziriq marsh in south of Iraq. Hydrology. https://doi.org/10.3390/hydrology6010021

Amin A, Iqbal J, Asghar A, Ribbe L (2018) Analysis of current and future water demands in the Upper Indus Basin under IPCC climate and socio-economic scenarios using a hydro-economic WEAP model. Water (Switzerland). https://doi.org/10.3390/w10050537

Arsiso B, Mengistu Tsidu G, Stoffberg GH, Tadesse T (2017) Climate change and population growth impacts on surface water supply and demand of Addis Ababa, Ethiopia. Clim Risk Manag 18(August):21–33. https://doi.org/10.1016/j.crm.2017.08.004

Asfaw A, Simane B, Hassen A, Bantider A (2018) Variability and time series trend analysis of rainfall and temperature in north-central Ethiopia: a case study in Woleka sub-basin. Weather Clim Extrem 19(June):29–41. https://doi.org/10.1016/j.wace.2017.12.002

Ayt Ougougdal H, Yacoubi Khebiza M, Messouli M, Lachir A (2020) Assessment of future water demand and supply under IPCC climate change and socio-economic scenarios, using a combination of models in Ourika watershed, High Atlas, Morocco. Water (Switzerland). https://doi.org/10.3390/w12061751

Bayable G, Amare G, Alemu G, Gashaw T (2021) Spatiotemporal variability and trends of rainfall and its association with Pacific Ocean Sea surface temperature in West Harerge Zone, Eastern Ethiopia. Environ Syst Res. https://doi.org/10.1186/s40068-020-00216-y

Bekele D, Alamirew T, Kebede A, Zeleke G, Melese AM (2017) Analysis of rainfall trend and variability for agricultural water management in Awash River Basin, Ethiopia. J Water Clim Change 8(1):127–141. https://doi.org/10.2166/wcc.2016.044

Bouznad IE, Elahcene O, Belksier MS (2020) Management model for water demand using the WEAP tool: case of Setif province-Algerian highlands. J Water Land Dev 45:19–28. https://doi.org/10.24425/jwld.2020.133042

Chaemiso SE, Abebe A, Pingale SM (2016) Assessment of the impact of climate change on surface hydrological processes using SWAT: a case study of Omo-Gibe River basin, Ethiopia. Model Earth Syst Environ. https://doi.org/10.1007/s40808-016-0257-9

Cheung WH, Senay GB, Singh A (2008) Trends and spatial distribution of annual and seasonal rainfall in Ethiopia. Int J Climatol 28(13):1723–1734. https://doi.org/10.1002/joc.1623

Das J, Mandal T, Rahman ATMS, Saha P (2021) Spatio-temporal characterization of rainfall in Bangladesh: an innovative trend and discrete wavelet transformation approaches. Theor Appl 143(3–4):1557–1579. https://doi.org/10.1007/s00704-020-03508-6

Descheemaeker K, Poesen J, Borselli L et al (2008) Runoff curve numbers for steep hillslopes with natural vegetation in semi-arid tropical highlands, northern Ethiopia. Hydrol Process 22(20):4097–4105. https://doi.org/10.1002/hyp.7011

Dong C, Schoups G, Van de Giesen N (2013) Scenario development for water resource planning and management: a review. Technol Forecast Soc Change. https://doi.org/10.1016/j.techfore.2012.09.015

Emami F, Koch M (2018) Agricultural water productivity-based hydro-economic modeling for optimal crop pattern and water resources planning in the Zarrine River Basin, Iran, in the wake of climate change. Sustainability (Switzerland). https://doi.org/10.3390/su10113953

Fanta SS (2022) Analysis of spatiotemporal rainfall variability and trend in Gilgel Gibe Watershed, Southwest Ethiopia: 1985–2017. Arab J Geosci. https://doi.org/10.1007/s12517-022-10053-1

Fanta SS, Feyissa TA (2021) Performance evaluation of HEC-HMS model for continuous runoff simulation of Gilgel Gibe watershed, Southwest Ethiopia. J Water Land Dev 50:85–97. https://doi.org/10.24425/jwld.2021.138185

Gebre SL (2015) Application of the HEC-HMS model for runoff simulation of Upper Blue Nile River Basin. J Waste Water Treat Anal. https://doi.org/10.4172/2157-7587.1000199

Gedefaw M, Wang H, Yan D et al (2019) Water resources allocation systems under irrigation expansion and climate change scenario in Awash River Basin of Ethiopia. Water (Switzerland). https://doi.org/10.3390/w11101966

George Marcellus Metobwa O (2018) Water demand simulation using WEAP 21: a case study of the Mara River Basin, Kenya. Int J Nat Resour Ecol Manag. https://doi.org/10.11648/j.ijnrem.20180301.12

Golmohammadi G et al (2014) Evaluating three hydrological distributed watershed models: MIKE-SHE, APEX. SWAT Hydrol 1(1):20–39. https://doi.org/10.3390/hydrology1010020

Gyawali R, Watkins DW (2013) Continuous hydrologic modeling of snow-affected watersheds in the Great Lakes Basin using HEC-HMS. J Hydrol Eng 18(1):29–39. https://doi.org/10.1061/(asce)he.1943-5584.0000591

Halwatura D, Najim MMM (2013) Application of the HEC-HMS model for runoff simulation in a tropical catchment. Environ Modell Softw 46:155–162. https://doi.org/10.1016/j.envsoft.2013.03.006

Hamed KH (2009) Enhancing the effectiveness of prewhitening in trend analysis of hydrologic data. J Hydrol 368(1–4):143–155. https://doi.org/10.1016/j.jhydrol.2009.01.040

Hussen B, Mekonnen A, Pingale SM (2018) Integrated water resources management under climate change scenarios in the sub-basin of Abaya-Chamo, Ethiopia. Model Earth Syst Environ 4(1):221–240. https://doi.org/10.1007/s40808-018-0438-9

Jaweso D, Abate B, Bauwe A, Lennartz B (2019) Hydro-meteorological trends in the upper Omo-Ghibe river basin, Ethiopia. Water (Switzerland). https://doi.org/10.3390/w11091951

Jillo AY, Demissie SS, Viglione A, Asfaw DH, Sivapalan M (2017) Characterization of regional variability of seasonal water balance within Omo-Ghibe River Basin, Ethiopia. Hydrol Sci J 62(8):1200–1215. https://doi.org/10.1080/02626667.2017.1313419

Koneti S, Sunkara SL, Roy PS (2018) Hydrological modeling with respect to impact of land-use and land-cover change on the runoff dynamics in Godavari River basin using the HEC-HMS model. ISPRS Int J Geo-Inf. https://doi.org/10.3390/ijgi7060206

Kumarasamy K, Belmont P (2018) Calibration parameter selection and watershed hydrology model evaluation in time and frequency domains. Water (Switzerland). https://doi.org/10.3390/w10060710

Li X, Zhao Y, Shi C, Sha J, Wang ZL, Wang Y (2015) Application of water evaluation and planning (WEAP) model for water resources management strategy estimation in coastal Binhai New Area, China. Ocean Coast Manag 106:97–109. https://doi.org/10.1016/j.ocecoaman.2015.01.016

Pedro-Monzonís M, Jiménez-Fernández P, Solera A, Jiménez-Gavilán P (2016) The use of AQUATOOL DSS applied to the System of Environmental-Economic Accounting for Water (SEEAW). J Hydrol 533:1–14. https://doi.org/10.1016/j.jhydrol.2015.11.034

Machiwal D, Gupta A, Jha MK, Kamble T (2019) Analysis of trend in temperature and rainfall time series of an Indian arid region: comparative evaluation of salient techniques. Theor Appl Climatol 136(1–2):301–320. https://doi.org/10.1007/s00704-018-2487-4

Majidi A, Shahedi K (2012) Simulation of rainfall-runoff process using Green-Ampt method and HEC-HMS model (case study: Abnama Watershed, Iran). Int J Hydraul 1(1):5–9. https://doi.org/10.5923/j.ijhe.20120101.02

Moriasi DN, Arnold JG, Van Liew MW, Bingner RL, Harmel RD, Veith TL (2007) Model evaluation guidelines for systematic quantification of accuracy in watershed simulations. Trans ASABE 50(3):885–900

Mourad KA, Alshihabi O (2016) Assessment of future Syrian water resources supply and demand by the WEAP model. Hydrol Sci J 61(2):393–401. https://doi.org/10.1080/02626667.2014.999779

Najim MMM, Babel MS, Loof R (2006) AGNPS model assessment for a mixed forested watershed in Thailand. Sci Asia 32:53–61. https://doi.org/10.1002/hyp.1344

Olabanji MF, Ndarana T, Davis N, Archer E (2020) Climate change impact on water availability in the olifants catchment (South Africa) with potential adaptation strategies. Phys Chem Earth 120(August):102939. https://doi.org/10.1016/j.pce.2020.102939

Oromiya Water Work Design and Supervision Enterprise Guideline (2010) https://www.scribd.com/document/483537419/Ethiopia-Design-Gudeline-Final-Oromia. Accessed 05 Mar 2020

Pechlivanidis IG, Jackson BM, Mcintyre NR, Wheater HS (2011) Catchment scale hydrological modelling: a review of model types, calibration approaches, and uncertainty analysis methods in the context of recent developments in technology and applications. Glob Nest J 13(3):193–214. https://doi.org/10.30955/gnj.000778 (**Accessed 29 May 2020**)

Pousa R, Costa MH, Pimenta FM, Fontes VC, Brito VFAD, Castro M (2019) Climate change and intense irrigation growth in Western Bahia, Brazil: the urgent need for hydroclimatic monitoring. Water (Switzerland). https://doi.org/10.3390/w11050933

Psomas A, Panagopoulos Y, Stefanidis K, Mimikou M (2017) Assessing future water supply and demand in a water-stressed catchment after environmental restrictions on abstractions. J Water Supply Res Technol AQUA 66(7):442–453. https://doi.org/10.2166/aqua.2017.130

Roozbahani R, Schreider S, Abbasi B (2015) Optimal water allocation through a multi-objective compromise between environmental, social, and economic preferences. Environ Modell Softw 64:18–30. https://doi.org/10.1016/j.envsoft.2014.11.001

Seleshi Y, Zanke U (2004) Recent changes in rainfall and rainy days in Ethiopia. Int J Climatol 24(8):973–983. https://doi.org/10.1002/joc.1052

Şen Z (2012) Innovative trend analysis methodology. J Hydrol Eng 17(9):1042–1046. https://doi.org/10.1061/(asce)he.1943-5584.0000556

Shumet AG, Mengistu KT (2016) Assessing the impact of existing and future water demand on economic and environmental aspects (case study from Rift Valley Lake Basin: Meki-Ziway Sub Basin), Ethiopia. Int J Waste Resour. https://doi.org/10.4172/2252-5211.1000223

Silva FB, de Almeida LT, de Oliveira Vieira E, da Silva DD, Maciel IP, Júnior FP (2020) Pluviometric and fluviometric trends in association with future projections in areas of conflict for water use. J Environ Manag. https://doi.org/10.1016/j.jenvman.2020.110991

Skhakhfa ID, Ouerdachi L (2016) Hydrological modelling of Wadi ressoul watershed, Algeria, by HEC-HMS model. J Water Land Dev 31(1):139–147. https://doi.org/10.1515/jwld-2016-0045

Sun SK, Li C, Wu PT, Zhao XN, Wang YB (2018) Evaluation of agricultural water demand under future climate change scenarios in the Loess Plateau of Northern Shaanxi, China. Ecol Indic 84(June 2017):811–819. https://doi.org/10.1016/j.ecolind.2017.09.048

Takala W, Adugna T, Tamam D (2016) The effects of land use land cover change on hydrological process of Gilgel Gibe, Omo Gibe Basin, Ethiopia. Int J Sci Eng Res 7(8):117–128

Tassew BG, Belete MA, Miegel K (2019) Application of HEC-hms model for flow simulation in the Lake Tana Basin: the case of Gilgel Abay Catchment, Upper Blue Nile Basin, Ethiopia. Hydrology. https://doi.org/10.3390/hydrology6010021 (**Accessed 23 Dec 2019**)

Teklu N, Talema A, Mogessie E (2016) Proceeding of the second national consultative workshop on integrated watershed management on Omo-Gibe Basin. https://www.researchgate.net/publication/313428353_Proceeding_of_The_Second_National_Consultative_Workshop_on_Integrated_Watershed_Management_of_Omo-Gibe_Basin. Accessed on: 17 May 2019

Tena TM, Mwaanga P, Nguvulu A (2019) Hydrological modelling and water resources assessment of Chongwe River Catchment using WEAP model. Water (Switzerland). https://doi.org/10.3390/w11040839

Touseef M, Chen L, Yang W (2021) Assessment of surfacewater availability under climate change using coupled SWAT-WEAP in Hongshui River Basin, China. ISPRS Int J Geo-Inf. https://doi.org/10.3390/ijgi10050298

United Nations Development Programme (2014) Communities in action for landscape resilience and sustainability the comdeks programme, p 152. https://satoyama-initiative.org/case_studies/comdeks-project-gilgel-gibe-catchment-ethiopia/. Accessed 26 June 2020

Verma AK, Jha MK, Mahana RK (2010) Evaluation of HEC-HMS and WEPP for simulating watershed runoff using remote sensing and geographical information system. Paddy Water Environ 8(2):131–144. https://doi.org/10.1007/s10333-009-0192-8

Wu D et al (2019) Reuse of return flows and its scale effect in irrigation systems based on modified SWAT model. Agric Water Manag

213(October 2018):280–288. https://doi.org/10.1016/j.agwat.2018.10.025

Yao AB, Mangoua OMJ, Georges ES et al (2021) Using "Water Evaluation and Planning" (WEAP) model to simulate water demand in Lobo Watershed (Central-Western Cote d'Ivoire)'. J Water Resour Prot 13(03):216–235. https://doi.org/10.4236/jwarp.2021.133013

Zelelew DG, Melesse AM (2018) Applicability of a spatially semi-distributed hydrological model for watershed scale runoff estimation in Northwest Ethiopia. Water (Switzerland) 10(7):10–12. https://doi.org/10.3390/w10070923

Zou KH, Tuncali K, Silverman SG (2003) Correlation and simple linear regression. Radiology 227(3):617–628. https://doi.org/10.1148/radiol.2273011499